PRE-SHUTTLE LIDAR SYSTEM RESEARCH

by

R.H. Lang and M.E. Zaghloul
Department of Electrical Engineering
and Computer Science
The George Washington University
Washington, D.C. 20052

Final Report
For the period April 1, 1984 through July 31, 1986

Prepared for the
National Aeronautics and Space Administration
Langley Research Center
Hampton, Virginia 23665

Under
Cooperative Agreement NCC1-85
John Wells, Technical Monitor
Flight Electronics Division

December 1986

PRE-SHUTTLE LIDAR SYSTEM RESEARCH

INTRODUCTION

This report describes the George Washington University ON CAMPUS technical support provided to NASA for the period April 1, 1984 through July 31, 1986 under cooperative agreement NCC1-85. The effort was performed by Faculty and Students in the Electrical Engineering and Computer Science (EE&CS) Department coordinated with NASA Langlely Research Center personnel.* Included are the results of the initial phase of a simulation study in connection with Photomultiplier Tubes (PMTs) and associated networks and an analytical investigation of the atmostpheric physics (including multiscattering) leading to modeling studies in connection with Differential Absorption Lidar (DIAL) observations. This effort was in support of the ER-2 aircraft DIAL projects. Part I of this report describes the photomulitplier tubes simulation studies by Professor M. E. Zaghloul# and Part II of this report describes the analytical modeling studies of the atmospheric physics by Professor R. H. Lang#.

---

*The authors are indebted to Robert Allen for his technical assistance and guidance.

#Professors Lang and Zaghloul are members of the Electrical Engineering and Computer Science Department, George Washington University, Washington, D.C.

PART I

PHOTOMULTIPLIER SIMULATION STUDIES

by

D.J. Rhee and M. E. Zaghloul

The George Washington University

Department of Electrical Engineering and Computer Science

Washington, D.C. 20052

ABSTRACT

In this project a computer model to simulate the nonlienar response of the PMT due to the associated voltage-divider circuit is developed. An equivalent circuit which approximates the operation of the device is first derived. This circuit is then used to develop the computer simulation model of the PMT. Simulation results are presented and discussed.

CONTENTS

PHOTOMULTIPLIER SIMULATION STUDIES

I. INTRODUCTION

Simulation studies were initiated to study the effect the loading of the voltage-divider circuit on the photomultiplier tube response. Under ideal conditions the response of the PMT is linear with respect to light flux, and approximately exponential with respect to applied voltage. In practice, however, the response of such a tube depends on the characteristics of the circuit supplying the required inter-electrode voltage [1], [2]. As a result nonlinearties occur because of "loading" effects in the associated circuitry. An accurate model of the PMT is useful in choosing a suitable method of compensation when a very high degree of linearity is required. For example, the choice of the value of the capacitors on the final dynode stages is critical to supply peak currents for each pulse received and to completely recover between returns. In this report we will describe efforts to develop computer simulations of typical PMT tube. The suggested RCA 7265 base (see published data sheet) was used in the simulation, although our approach is quite general and can be applied to any type of voltage divider network used for photomultiplier tube.

In this report we will develop mathematical models for PMT and PMT networks divider. Initial computer simulation are used for the PMT with "flat top" pulses. The light inputs are a pulse pair. A study is made of the effect of the first pulse on the second pulse.

II. EQUIVALENT CIRCUIT MODEL FOR PMT

To simulate the PMT and its associated voltage-divider network it was necessary to obtain an equivalent circuit model which approximates the behavior of the tube under operation. To illustrate the model used, consider the simplest voltage divider network for a multiplier tube as shown in Figure 1. This model of Figure 1 is simpler than the RCA 7265 model, however, it is used here to explain the theory. The standard tube-circuited notation is used where K is the photocathode, D_1, D_2,..., are dynodes, A is the anode, R_L is the anode load resistance. The resistors R_1, R_2,... are dynodes network resistors. For simplicity the currents shown are "electron currents" rather than conventional currents which flow in opposite directions.

From Figure 1, let cathode current be I_k and anode current be I_A. Assuming the currents in dynodes as shown, therefore

$$I_o = I_k + I_1 \tag{1}$$

$$I_1 = I_2 + I_{D1} \tag{2}$$

$$I_2 = I_3 + I_{D2} \tag{3}$$

$$I_n = I_{n+1} + I_{Dn} \tag{4}$$

$$I_o = I_{n+1} + I_A \tag{5}$$

In general

$$I_n = I_{n+1} + I_{Dn} \tag{6}$$

In the practical model RCA 7265 shown in Figure 2 of the data sheet, we have 14 dynodes, i.e. n = 14. Also, there are capacitors starting at n = 10.

Therefore, in this case we have

$$I_{10} = I_{11} + I_{c1} + I_{D10}$$

$$I_{11} = I_{12} + I_{c2} + I_{D11}$$

$$I_{12} = I_{13} + I_{c3} + I_{D12}$$

$$I_{13} = I_{14} + I_{c4} + I_{D13}$$

$$I_{14} = I_{15} + I_{c5} + I_{D14}$$

$$I_0 = I_{15} + I_{c5} + I_A$$

Due to secondary emission [3], [4], [5], current at each dynode D_i must supply a secondary emission current to the next dynode g times larger than the current incident to it.

From Figure 1 the current supplied to the last dynode is:

$$I_{Dn} = I_A - I_A/g = I_A(1 - 1/g) = I_A(1-r) \qquad (7)$$

where r = 1/g is the ratio of the currents, i.e. the stage gain. Assuming, for simplicity, equal current gain ratio at each stage, we have in general:

$$I_{Di} = I_A r^{(n-i)(1-r)} \qquad (8)$$

$$I_k = I_A r^n = I_A/G \qquad (9)$$

where $G = r^n$ is overall gain of the multiplier. It follows from (8) that

$$I_{D1} = gI_k - I_k \qquad (10)$$

Let $\hat{I}_1 = gI_k$

$$\therefore I_1 = I_{D1} + I_k \qquad (11)$$

Similarly

$$I_{D2} = I_A r^{n-2}(1-r)$$

$$= I_k g^2(1-1/g) = g\hat{I}_1 - I_1$$

Let $g\hat{I}_1 = I_2$

$$\therefore \hat{I}_2 = I_{D2} + I_1 \tag{12}$$

and so on for all other stages. Therefore, each successive current gain in each dynode stage is represented by a current source as shown in Figure 3. We note that in general the current gain ratio at each dynode stage is proportional to the voltage applied to it and it changes from one stage to another.

III. CURRENT GAIN BEHAVIOR

The secondary-emission process, which is fundamental to photomultipliers can be considered to consist of three physical processes (1) excitation of secondary electron (2) transport of these electrons through the solid and (3) transport though the vacuum-solid interface. In elementary theory of secondary emission it is assumed that the secondary emission yield δ defined as the ratio of secondary to primary current is function of the primary energy [4], that is

$$\delta = \int n(x_1, E_o)\, f(x)\, dx$$

where: $n(x_1, E_o)$ is the number of secondary electrons produced at distance x_1 from the surface by a primary electron of energy E_o. $f(x)$ is the probability that a secondary electron produced

at x reaches surface and is emitted in vacuum.

Both the theoretical and experimental evidence [1], [3], [4], suggest that we can represent the stage gain g as power law in the accelerating voltage v

$$\therefore g = Av^p \tag{13}$$

where

A is constant depends on the material used in the tube manufacture

p is constant generally ≤ 1

The constants A and p are generally determined from the tube manufacturer supplied curves. General discussions on the constants A and B are also found in [5]. For a tube with n identical stages, the overall tube voltage is

$$V = (n+1)v \tag{14}$$

The overall gain of the tube is

$$G = g^n = (Av^p)^n = A^n \left[\frac{V}{(n+1)} \right]^{np}$$

$$= BV^q$$

where $q = np$ or $p = q/n$, and

$$q = d(\log G)/d(\log V) \tag{15}$$

$$B = A^n/(n+1)^{np}$$

For a practical tube, empirical gain-voltage curve could be used and hence, we can obtain q and p. Figue 4 of RCA 7265 data sheet was used to determine the constants A and p.

From Figure 4 of the data sheet, it follows:

$$p = 0.8556 \tag{16}$$

$$A = 0.0448 \tag{17}$$

We used the above data in simulating the PMT. For the given PMT RCA 7265 with n = 14 and from data sheet the overall gain obtained from the data sheet is:

$$G = 4.8 \times 10^7$$

Therefore, the gain g per each stage is

$$g = \sqrt[14]{4.8 \times 10^7} = 3.53$$

Therefore, each stage has equal gain of 3.53.

This, of course, is oversimplified as discussed above and a more accurate model for each stage i is

$$g_i = Av_i^p \tag{18}$$

where A and p are as given by (16), and (17) and v_i is the voltage across each dynode stage. We developed our algorithm based on Equation (18). Thus, in our results the gain g_i per each stage depends on the accelerating volage of each stage.

IV. COMPUTER SIMULATION

The circuit shown in Figure 3 is a nonlinear circuit, which has nonlinear components such as the Zener diodes shown and nonlinear controlled sources which represents the current gain. A study of the linearity response of PMT and its relation to the network of resistors can be found in [6,7]. The component values of circuit of Figure 3 were obtained from the data sheet of the RCA 7265 with 2400 volt power supply. In the simulation effort we were interested to obtain the variation of the anode current versus time and the variation of any other variable in the circuit. Each dynode gain current is

represented by nonlinear current source, where its value is a function of the voltage across it as in Equation (18). The circuit of Figure 3, in general, is governed by nonlinear differential equations which are to be solved at each time step to obtain the response at various instants of time. Because of that, the general nonlinear simulation technique [8,9], may be used for simulation. In our effort, general equations were obtained in terms of the circuit parameters, and several cases were studied for different parameters. To obtain the cathode current, consider, for example, the two cases of the average photons arrival rate (# photons/sec) I_p:

i) I_p = 2000 photons/μS

ii) I_p = 200,000 photons/μS

Assume quantum efficiency = 0.1 at 532 nm, therefore, the average number of photoelectrons/sec is

$$I_{pe} = \eta I_p$$

For the above two cases we have

i) I_{pe} = 200 photoelectrons/μS

ii) I_{pe} = 20,000 photoelectrons/μS

and cathode current

$$I_k = I_{pe} * e$$

where e is the electron charge = 1.602E - 19 coulomb

Therefore

i) I_k = 3.2E-11 Amp

ii) I_k = 3.2E-09 Amp

V. RESULTS AND DISCUSSION

For the following results, we assumed that the amplification process is noise free, that all of the current emitted from the cathode is collected by the first dynode, and that the seconary emission ratio per stage is represented by (18). We used RCA 7265 with its voltage - divider network, and data as shown in Fig. 8 of RCA 7265 data sheet.

1. Simulation of voltage variations across R_L (load resistance) with High Voltage Power Supply (HVPS) of - 2400 VDC with Loading Capacitance C_5 = 500 PF

A wavelength of 532 nm was considered. The light pulses on the face of the PMT of 200 to 200,000 photons per microsecond (μS) were used in the simulation. The light input is flat pulse pair (on-line pulse followed by an off-line pulse) recurring every 100 μs (10 HZ). Both the on- and off-line pulses were the same with a flat top, a width of 20 μS and a separation of 200 μS. Figure 4 shows the pulse applied. The capacitor C_5 = 500 PF. The pulse output across the load R_L is shown in Figure 5 for case of 200 photon per μS. Figures 6 and 7 shows the pulse output across load resistance R_L for case of 2000 and 200,000 photons per μS. In the last case the results shows distortion. Table 1 shows the maximum anode voltage across the load resistor R_L versus different average photons arrival rate I_p in the interval of 200 -200,000 photons per μS. A plot of this voltage versus I_p is shown in Figure 8, for the case of first pulse followed

by second pulse. The results of Figure 8 shows that the difference between first and second pulse behaves as nonlinear function of cathode current as the light density increases.

2. Simulation of voltage variation across R_L with HVPS voltage - 2400 VDC with C_5 = 1000 PF and C_5 = 0.01 μF

Next, we changed the value of the loading capacitor C_5 to 1000 PF and then to 0.01 μF. The other loading capacitors in the PMT network are changed in ratio of C_5 as in the RCA data sheet. Figure 9 shows the voltage across R_L (V_{R_L}) for light density of 200 photon/μS and C_5 = 1000 PF. Figure 10 shows the voltage across R_L(V_{R_L}) for light density of 2000 photons/μS and C_5 = 1000 PF. Figure 11 shows the voltage across R_L (V_{RL}) for light density of 200,000 photons/μS and C_5 = 1000 PF. Similarly, the voltage across R_L for different light density and for C_5 = 0.01 μF are shown in Figures 12, 13, and 14, respectively. Tables 2 and Table 3 show the maximum anode voltage versus different average photons arrival rate I_p in the interval of 200 - 200,000 photons/μS for C_5 = 1000 PF and C_5 = 0.01 μF. A plot of such voltage is shown in Figure 15 and in Figure 16.

3. Simulation of the effect of the first pulse on the second pulse.

To determine the effect of the first pulse on the second pulse, the flat pulse width was increased from 20 μS to 100 μS. Figures 17, 18, and 19 show that the voltage across R_L for different values of

photons/μS and with C_5 = 500 PF. The results show that the pulse width variations do not affect the voltage variations across R_L, where the maximum value is the same as obtained before.

In all of the above simulation results it is clear that the PMT shows a nonlinear relation in the dynode voltages of the tube. This is because the secondary emission ratio depends on the voltage across each stage in the tube. It appears that as the number of photons/MS increases, and hence I_K increases the nonlinearity increases. In fact, the results show that an increase of light density more than 4000 photons/μS causes the difference between the first and second pulse to behave as a nonlinear function of cathode current. All of the above results were simulated for flat top pulse. Further simulations for exponentially decaying pulse are needed, where a study of the effect of the first pulse on the second pulse should be examined.

Additional information on PMT performance can be easily obtained using our developed simulation technique. For example, selecting optimum PMT components in the divider network and operating anode current for maximum linearity. Also, it is possible to use this technique to determine the dynode voltage change versus PMT gain. Our technique can be used with simple extentions in simulating PMT with transistor and Zener type bases or mixture of these. The above results are the initial phase of the simulation studies of PMT. Further studies as second phase of the above results are needed to complete the goal of the simulation.

VI. Recommendations for Further Study

To fully meet the objectives of the research project, it is recommended that a second phase of the simulation study be performed, specifically to accomplish:

1) Simulation for exponentially decaying pulse with recurring rates, photon arrival rates, wavelengths, turn-on delays, etc. Associated with the actual LaRc Electra DIAL observation. Also studying the PMT gain variation by selecting HVPS setting over the range used on the Electra DIAL project.

2) Selecting optimum PMT components in the divider network for maximum linearity of PMT operation.

3) Modify simulation model to include transistor base models. In this case simple extensions are to be added to the suggested simulation model. An improved base design should result from the simulation studies.

References:

[1] K. Sekkowski, Methods of Experimental Physics, Academic Press, New York 1974.

[2] R.W. Engstrom and E. Fischer, "Voltage-Divider Characteristics on Multiplier Phototube Response", The Review Scientific Instrument, Vol. 28, No. 7, July 1957.

[3] RCA Photomultiplier Manual, RCA, Harrison, NY, 1980.

[4] R.E. Simon and B.G. Williams, "Secondary - Electron Emission", IEEE Trans. Nucl. Sci. NS - 15, No. 3, June, 167, 1968

[5] P. L. Land, "A Discussion of the Region of Linear Operation of Photomultipliers", The Review of Scientific Instruments, Vol. 42, No. 4, April 1971.

[6] H. J. Lush, "Photomultiplier Linearity", Journal of Scientific Instrumentation, Vol. 42, 1965.

[7] G. Sauerbrey; "Deviation from Linearity in the Measurements of Radiation with Photomultipliers", App. Optics, 11, No. 11, 1973

[8] L. Chua, Computer Aided Designs and Algorithms, McGraw Hill, 1975

[8] A. Vladimirescu, K. Zhang, A.R. Newton, D.O. Peterson, and A. Sangiovanni-Vincartelli, Spice User's Guide, University of California, Berkeley, August 1981

APPENDIX I

LIST OF TABLES

LIST OF FIGURES

Figure 11: Output pulse across R_L, C_5 = 1000 PF, 200,000 photons/μs

Figure 12: Output pulse across R_L, C_5 = 0.01 μF, I_p = 200 photons/μs

Figure 13: Output pulse across R_L, C_5 = 0.01 μF, I_p = 2000 photons/μS

Figure 14: Output pulse across R_L, C_5 = 0.01 μF, I_p = 200,000

Figure 15: Maximum voltage across anode, C_5 = 1000 PF

Figure 16: Maximum voltage across anode, C_5 = 0.01 μF

Figure 17: Output voltage across R_L, C_5 = 500 PF, I_p = 200 photons/μS

Figure 18: Output voltage across R_L. C_5 = 500 PF, I_p = 2000 photons/μS

Figure 19: Output voltage across R_L, C_5 = 500 PF, I_p = 200,000 photons/μS

Table 1

Maximum Anode Voltage for 200-200,000 Photons/μS

Photons	Maximum Anode Voltage	Pulse #
200	7.68 E-03	1
	7.68 E-03	2
300	1.56 E-02	1
	1.56 E-02	2
800	3.23 E-02	1
	3.23 E-02	2
1,600	6.98 E-02	1
	6.98 E-02	2
2,000	9.09 E-02	1
	9.09 E-02	2
6,000	7.81	1
	6.8	2
10,000	2.49	1
	3.41	2
12,000	2.05	1
	2.11	2
18,000	3.73	1
	3.64	2
20,000	8.19	1
	7.36	2
80,000	1.20	1
	11.1	2
100,000	1.02	1
	6.41	2
180,000	1.41	1
	4.33	2
200,000	4.68	1
	3.76	2

Table 2

Maximum Voltage Across Anode - C_5 = 1000 PF

Photons	Maximum Anode Voltage	Pulse #
200	7.6 E-03	1
	7.6 E-03	2
600	2.3 E-02	1
	2.3 E-02	2
1,200	4.8 E-02	1
	4.8 E-02	2
1,600	6.6 E-02	1
	6.6 E-02	2
2,000	8.5 E-02	1
	8.5	8.5 E-02
6,000	3.5 E-01	1
	3.5 E-01	2
10,000	1.082	1
	1.108	2
14,000	3.96	1
	4.71	2
18,000	5.85	1
	6.17	2
20,000	3.146	1
	3.543	2
60,000	5.818	1
	7.1	2
100,000	14.2	1
	30.6	2
140,000	2.74	1
	3.14	2
180,000	2.50	1
	2.39	2
200,000	2.621	1
	2.448	2

Table 3

Maximum Voltage Across Anode, C_5 = 0.01 μF

Photons	Maximum Anode Voltage	Pulse #
200	7.57 E-03	1
	7.58 E-03	2
600	2.28 E-02	1
	2.28 E-02	2
1,200	4.59 E-02	1
	4.61 E-02	2
1,600	6.14 E-02	1
	6.18 E-02	2
2,000	7.71 E-02	1
	7.77 E-02	2
6,000	2.41 E-01	1
	2.47 E-01	2
10,000	4.18 E-01	1
	4.40 E-01	2
14,000	6.15 E-01	1
	6.60 E-01	2
18,000	8.29 E-01	1
	9.16 E-01	2
20,000	9.45 E-01	1
	1.061	2
60,000	6.21	1
	21.04	2
100,000	25.7	1
	28.3	2
140,000	25.8	1
	57	2
180,000	46	1
	3.85	2
200,000	22	1
	57.04	2

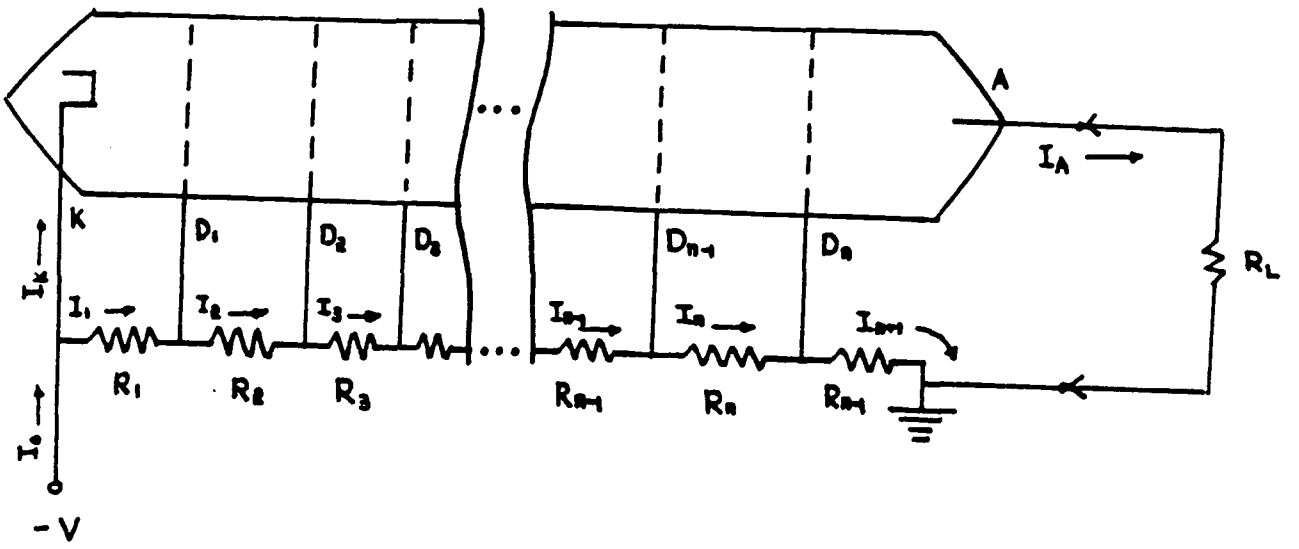

Figure 1

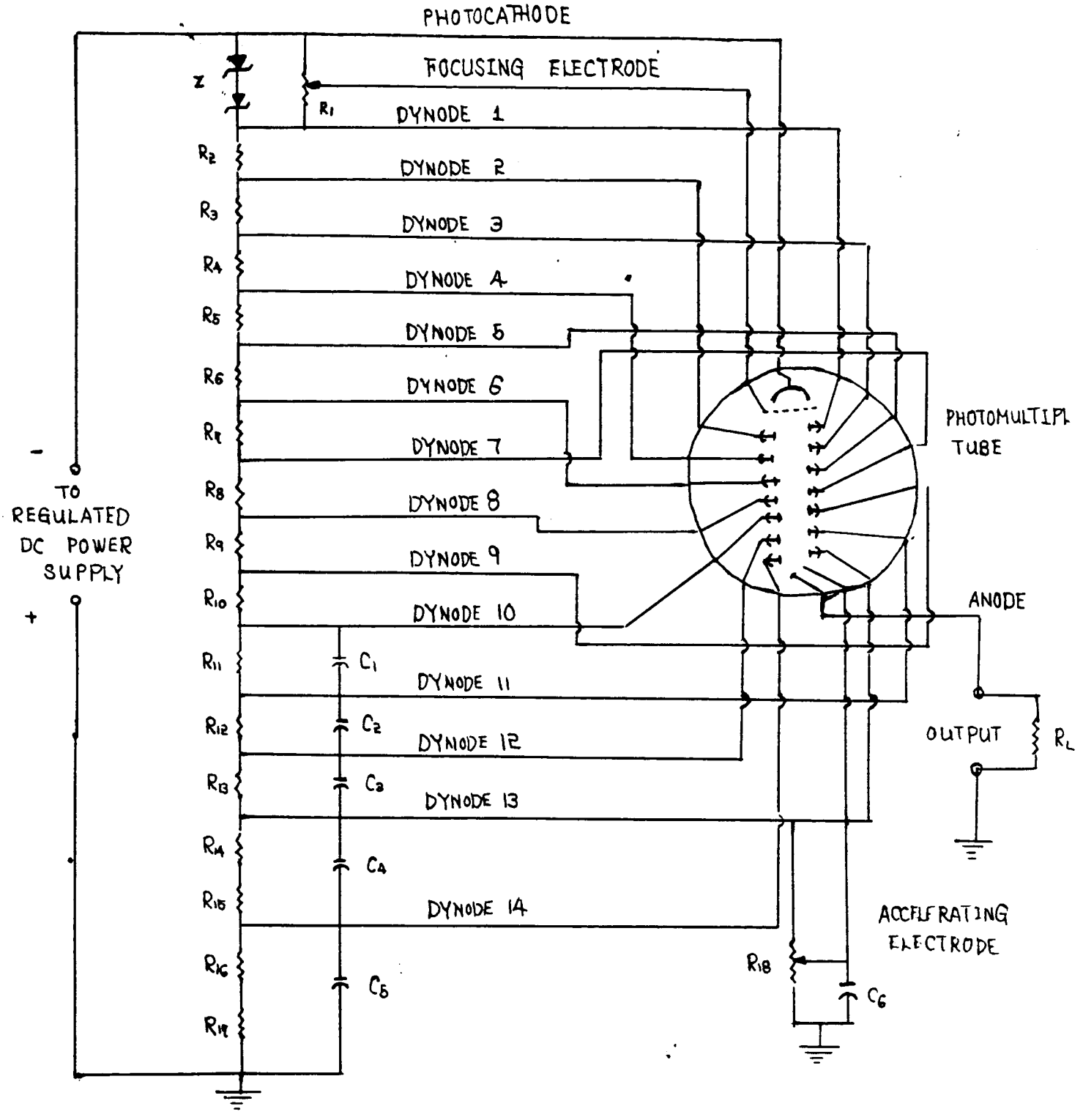
PHOTOCATHODE
FOCUSING ELECTRODE
Z
R1
DYNODE 1
R2
DYNODE 2
R3
DYNODE 3
R4
DYNODE 4
R5
DYNODE 5
R6
DYNODE 6
R7
DYNODE 7
R8
DYNODE 8
R9
DYNODE 9
R10
DYNODE 10
R11
C1
DYNODE 11
R12
C2
DYNODE 12
R13
C3
DYNODE 13
R14
C4
R15
DYNODE 14
R16
C5
R17
R18
C6
ACCELERATING ELECTRODE
PHOTOMULTIPLIER TUBE
ANODE
OUTPUT
RL
TO REGULATED DC POWER SUPPLY
-
+

Figure 2

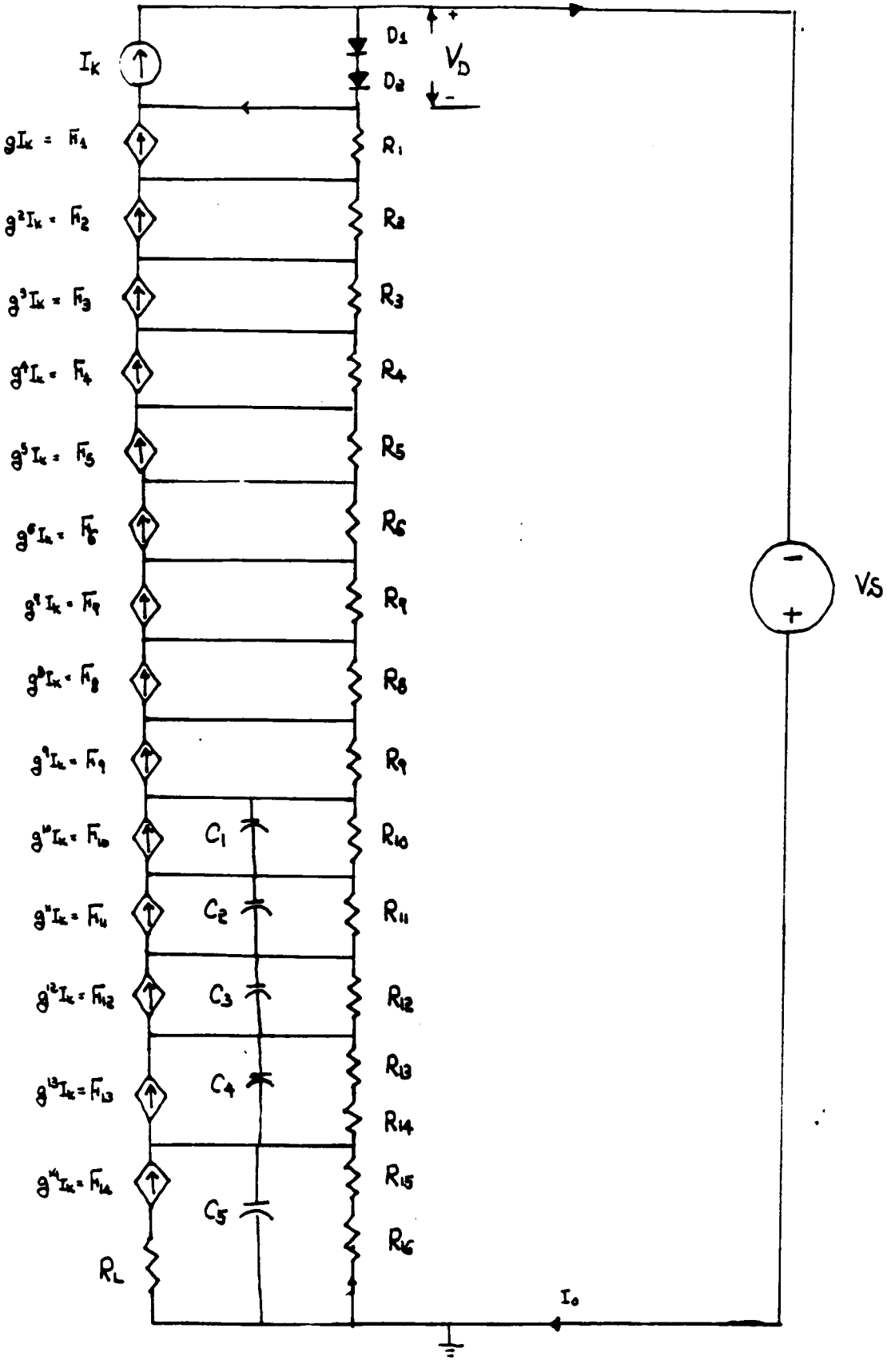
I_K
D_1
D_2
V_D
+
-
$gI_K = F_1$
$g^2I_K = F_2$
$g^3I_K = F_3$
$g^4I_K = F_4$
$g^5I_K = F_5$
$g^6I_K = F_6$
$g^7I_K = F_7$
$g^8I_K = F_8$
$g^9I_K = F_9$
$g^{10}I_K = F_{10}$
$g^{11}I_K = F_{11}$
$g^{12}I_K = F_{12}$
$g^{13}I_K = F_{13}$
$g^{14}I_K = F_{14}$
R_L
R_1
R_2
R_3
R_4
R_5
R_6
R_7
R_8
R_9
R_{10}
R_{11}
R_{12}
R_{13}
R_{14}
R_{15}
R_{16}
C_1
C_2
C_3
C_4
C_5
VS
I_o

Figure 3

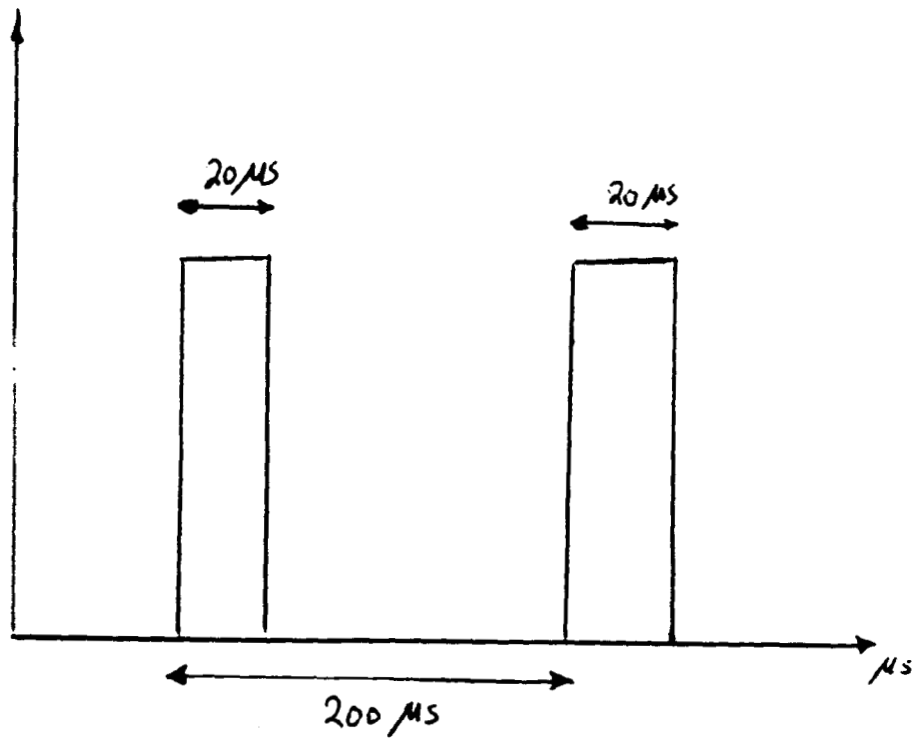

Figure (4)

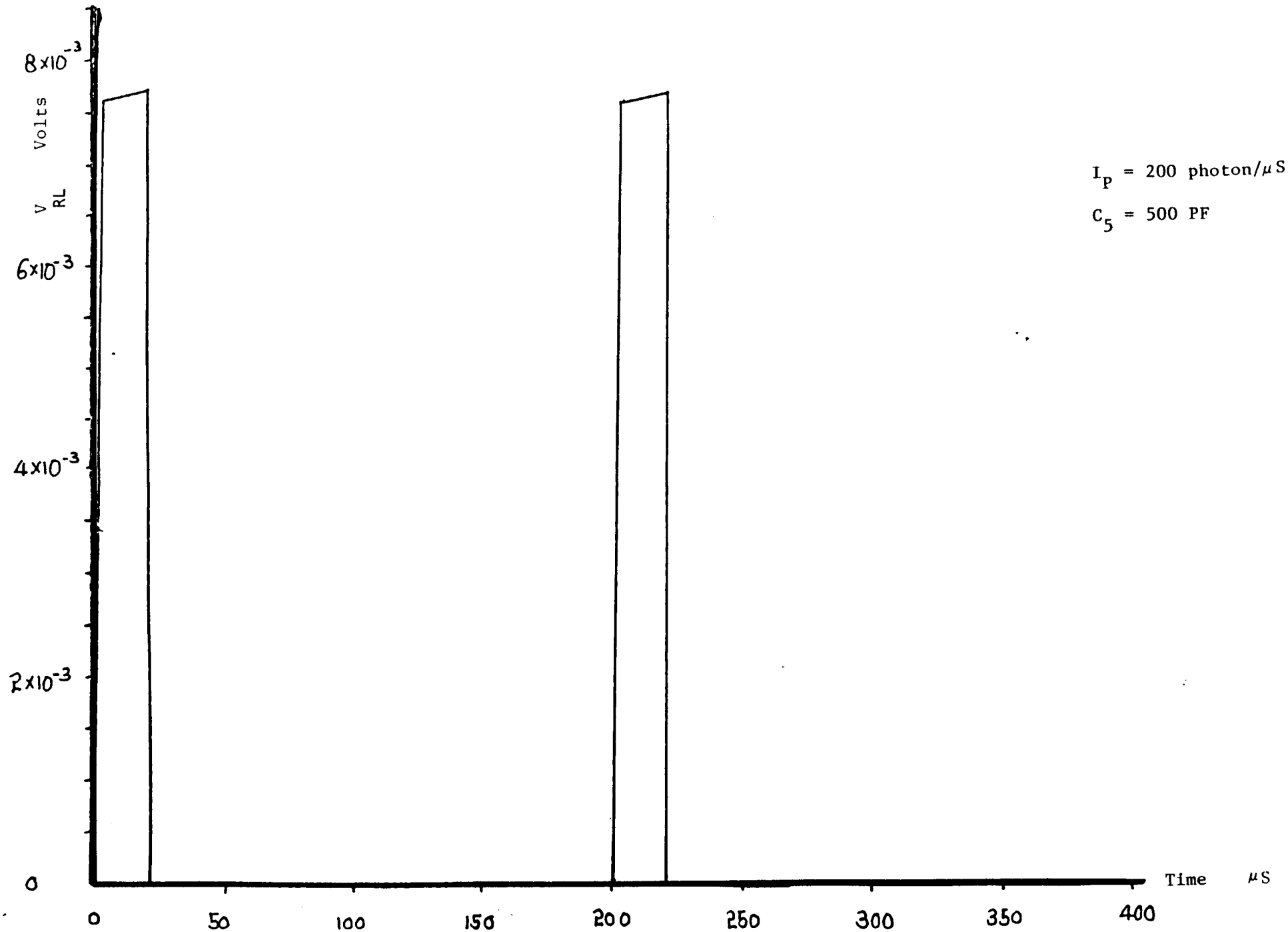

Figure 5 - Output Pulse Across R_L,
C_5 = 500 PF, I_P = 200 photons/μS

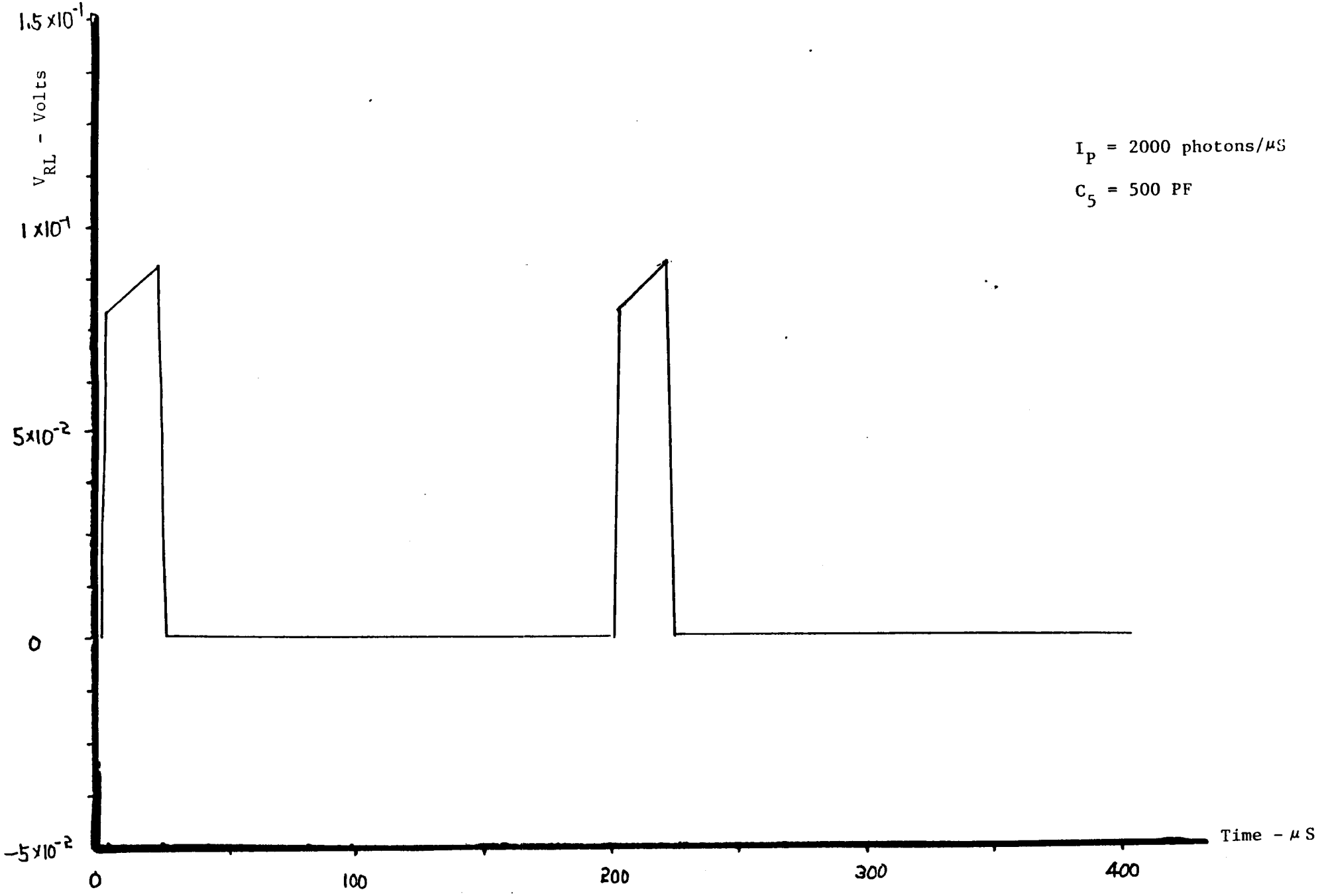

Figure 6 - Output Pulse Across R_L, C_5 = 500 PF, I_P = 2000 photons/μS

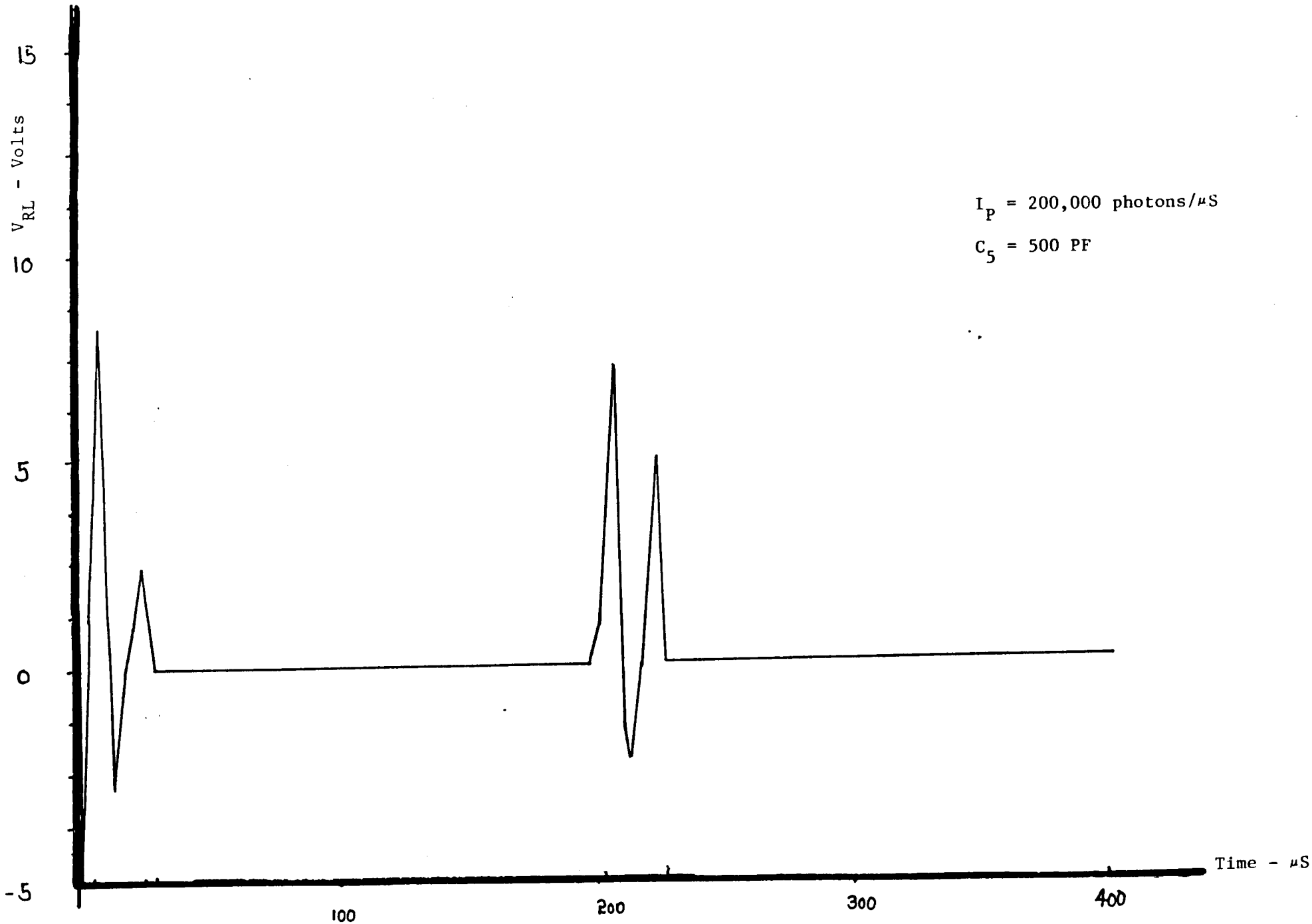

Figure 7 - Output Pulse Across R_L, C_5 = 500 PF, I_P = 200,000 photons/μS

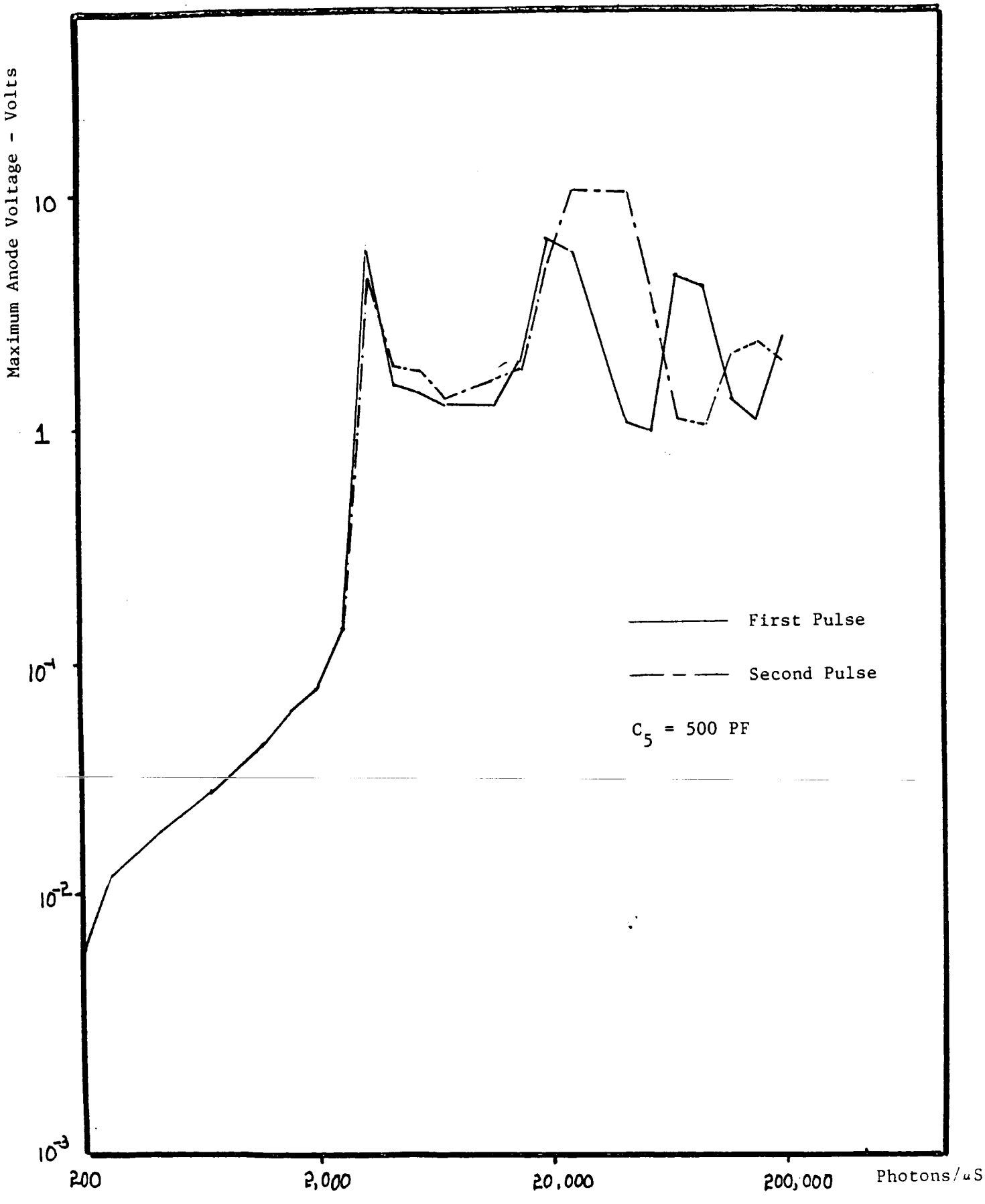

Figure 8 - Maximum Anode Voltage - Photons/μS

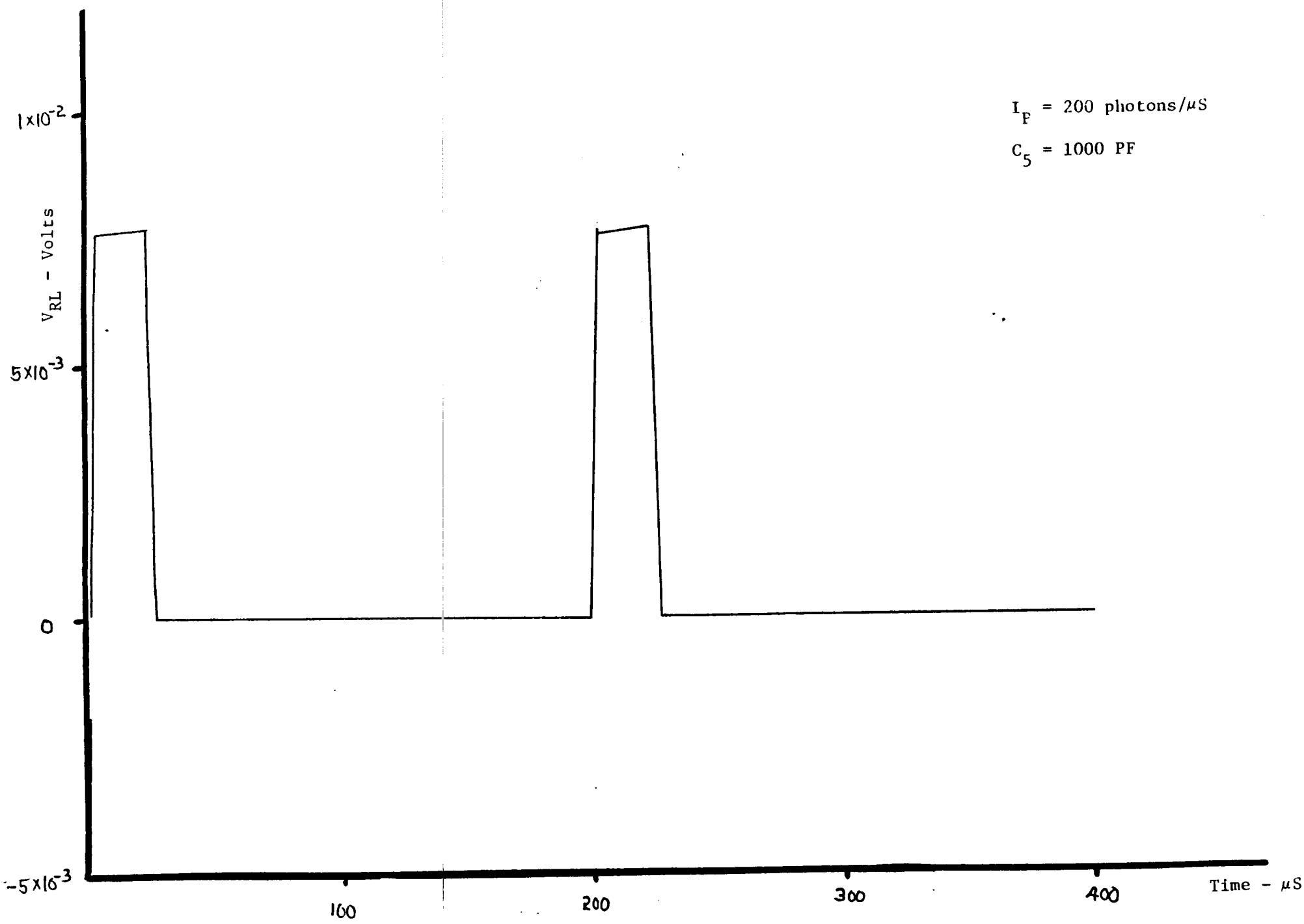

Figure 9 - Output Pulse Across R_L

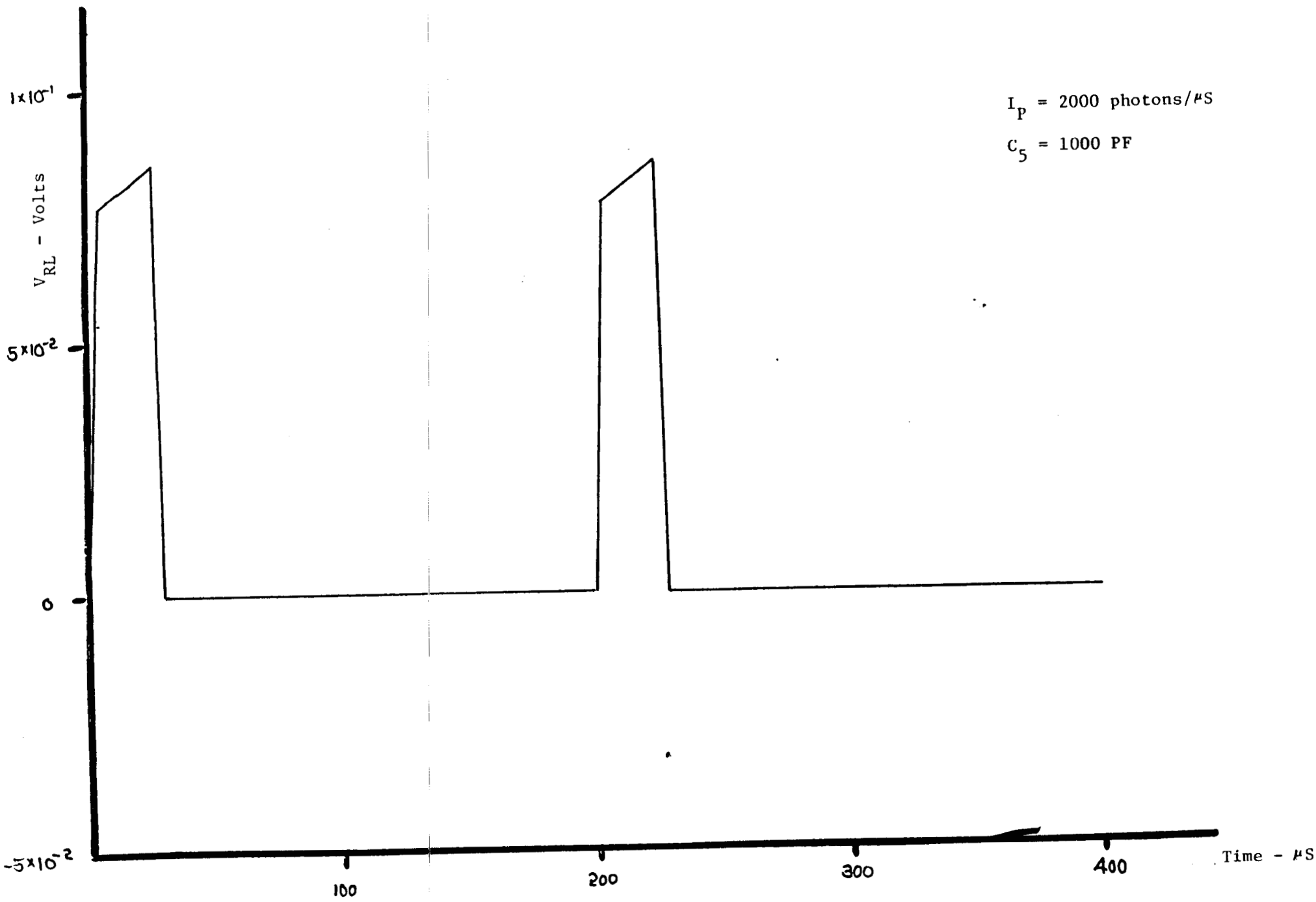

Figure 10 - Output Pulse Across R_L

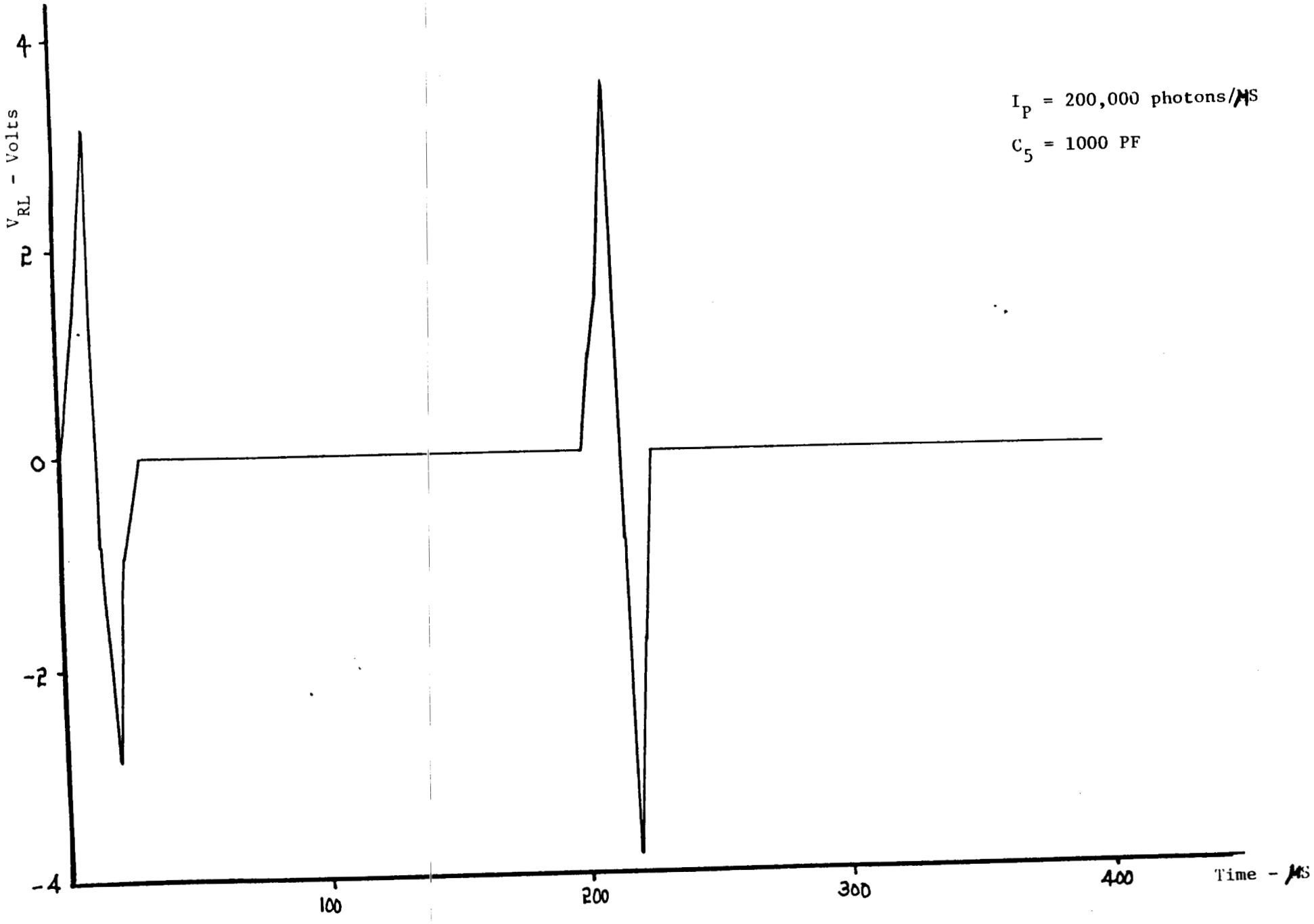

Figure 11 - Output Pulse Across R_L

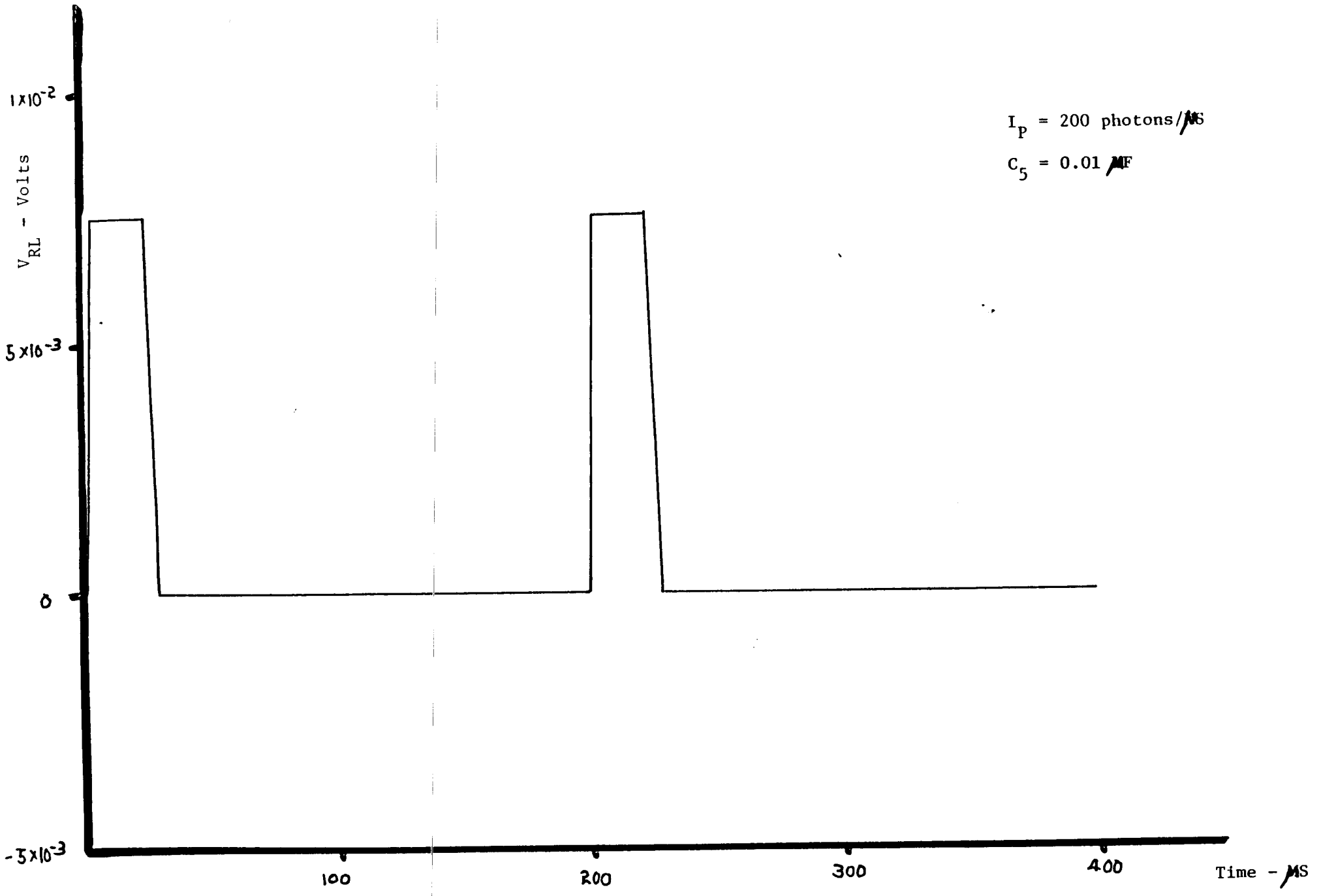

Figure 12 - Output Pulse Across R_L

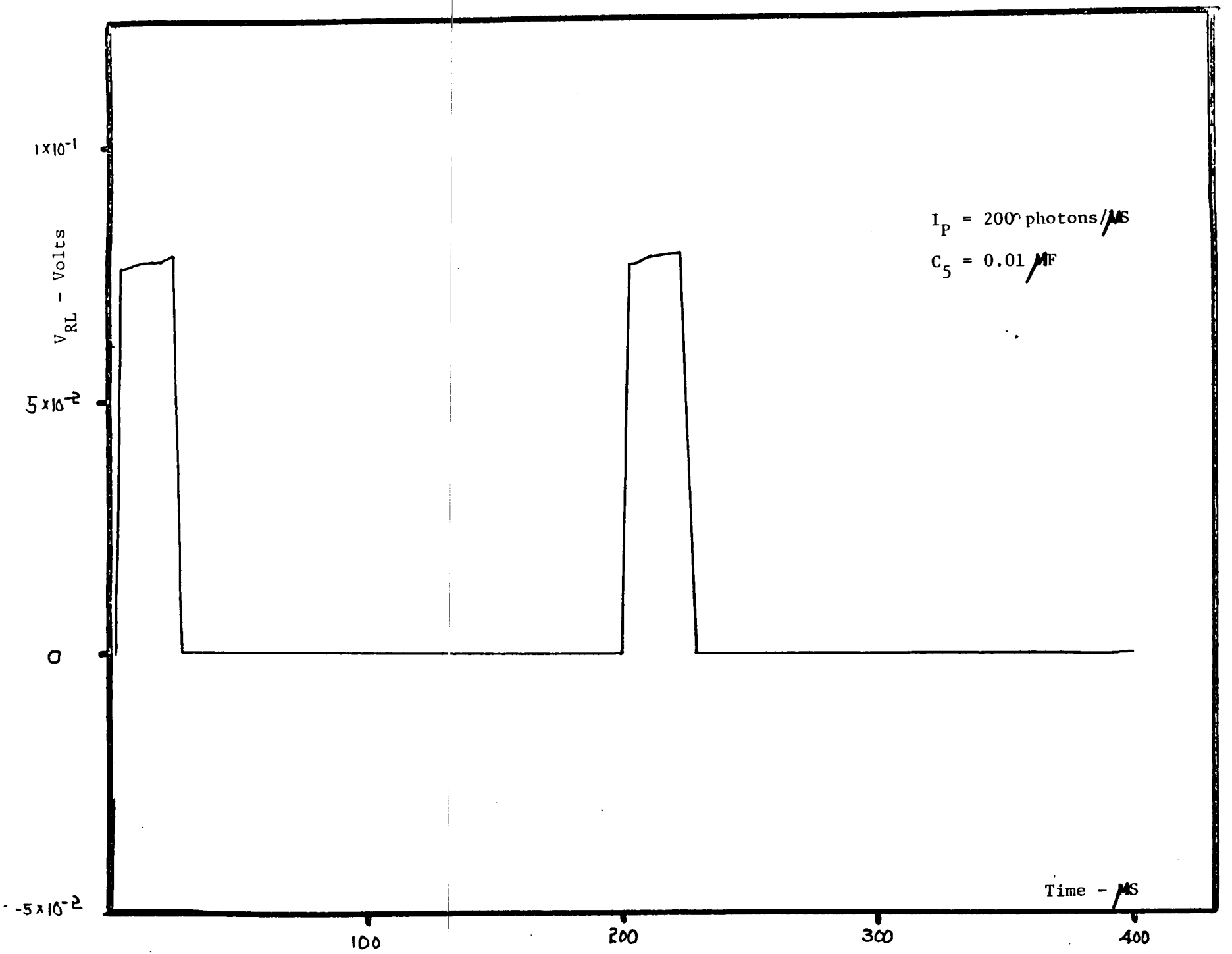

Figure 13 - Output Pulse Across R_L

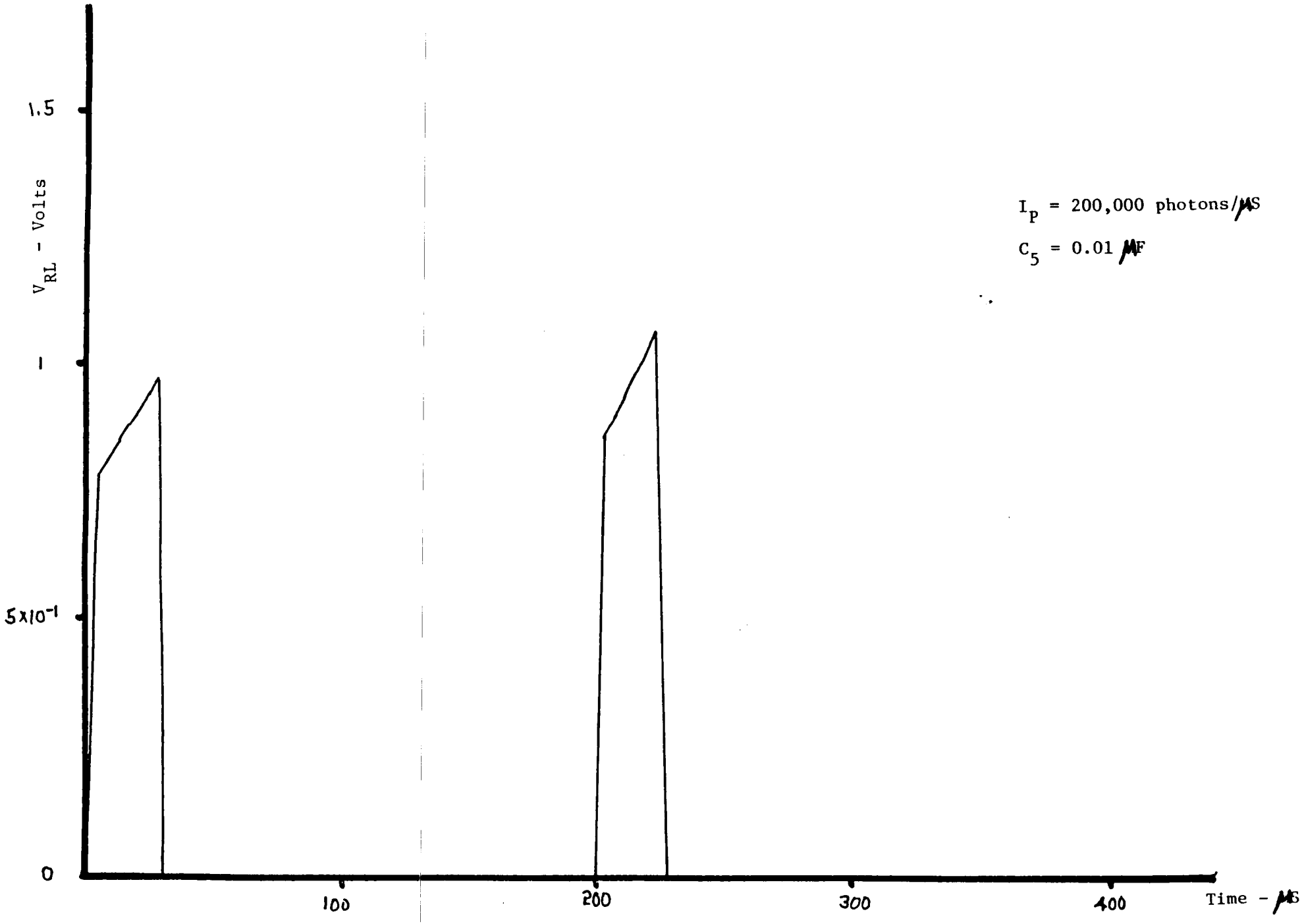

Figure 14 - Output Pulse Across R_L

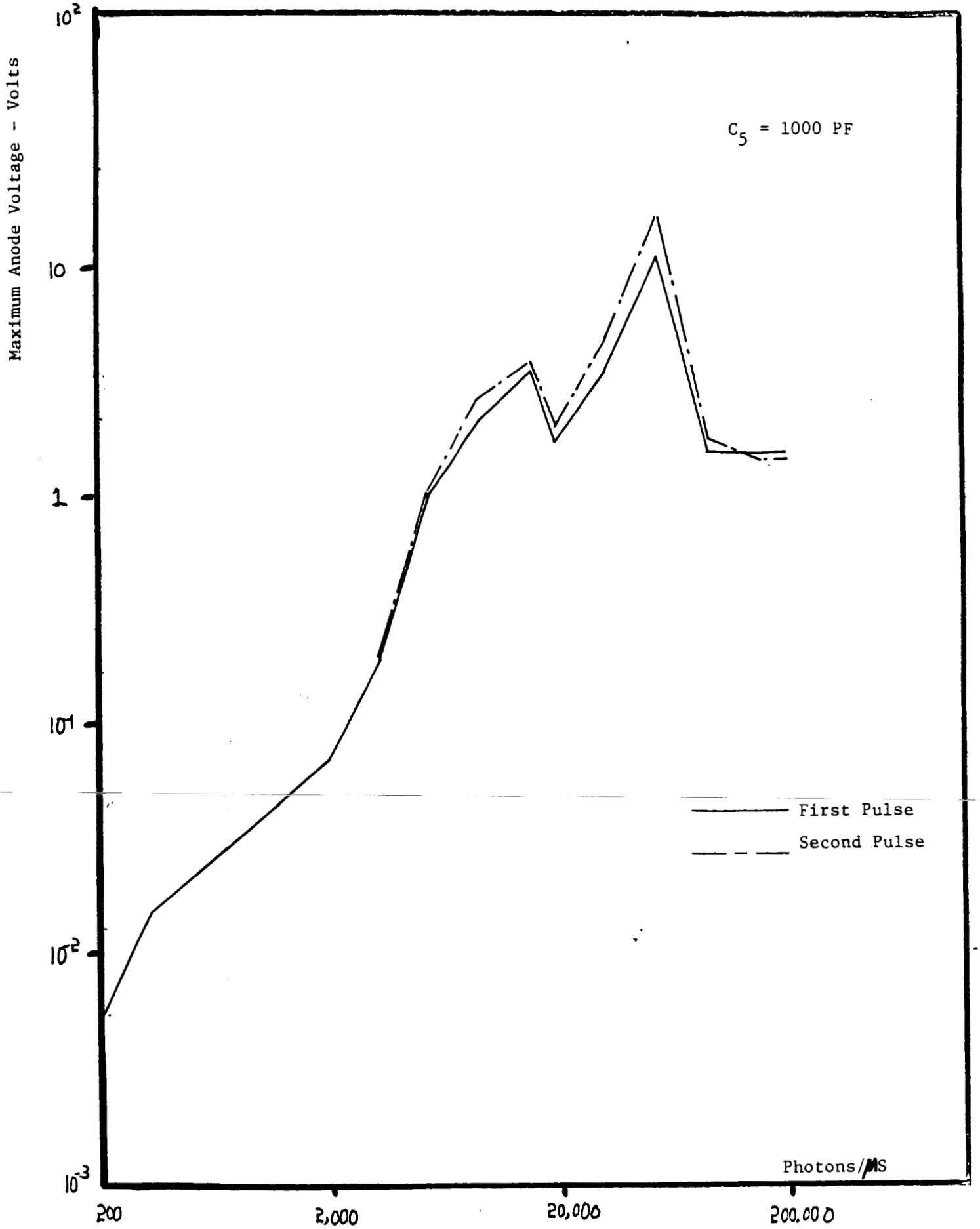

Figure 15 - Maximum Voltage Across Anode

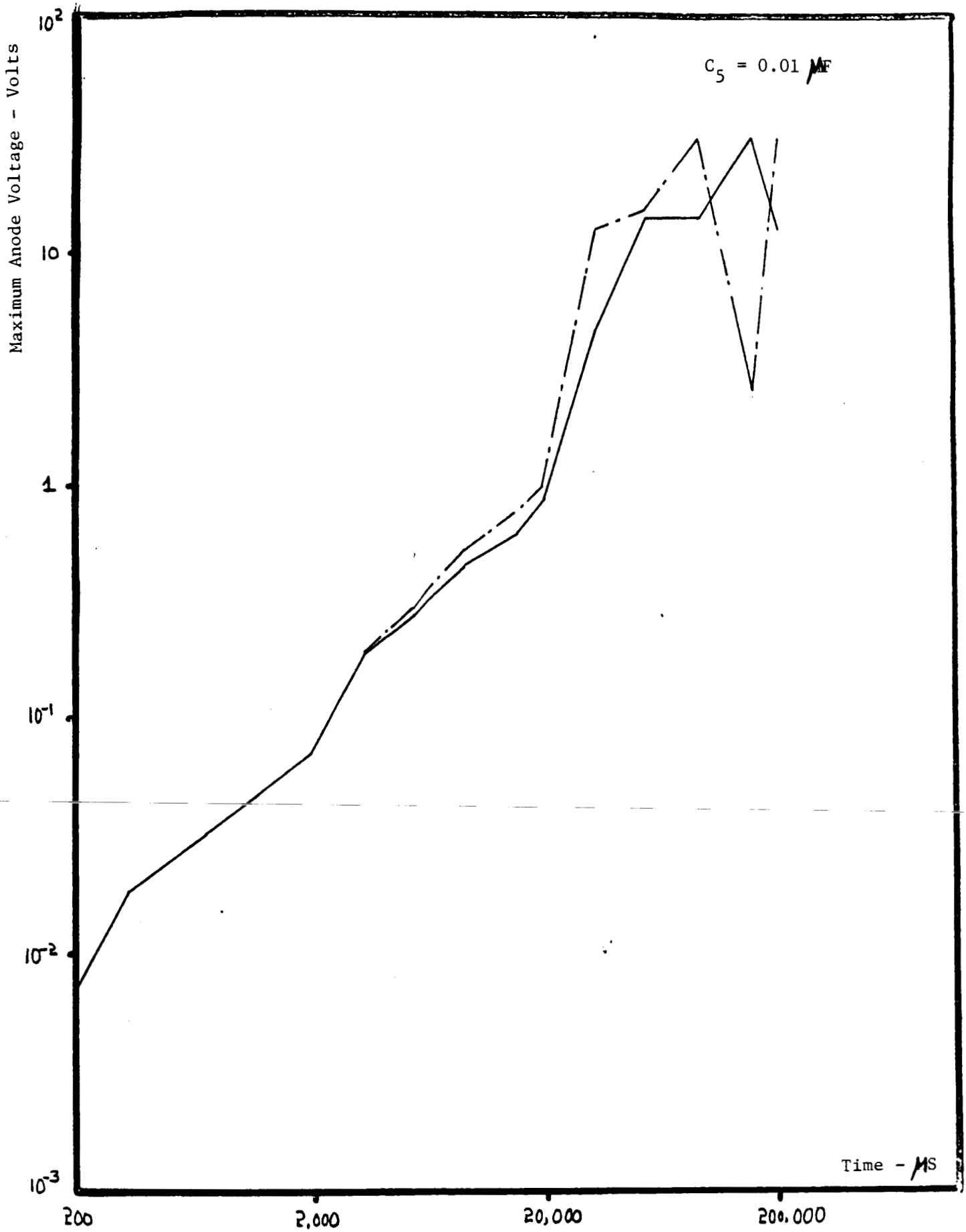

Figure 16 - Maximum Voltage Across Anode

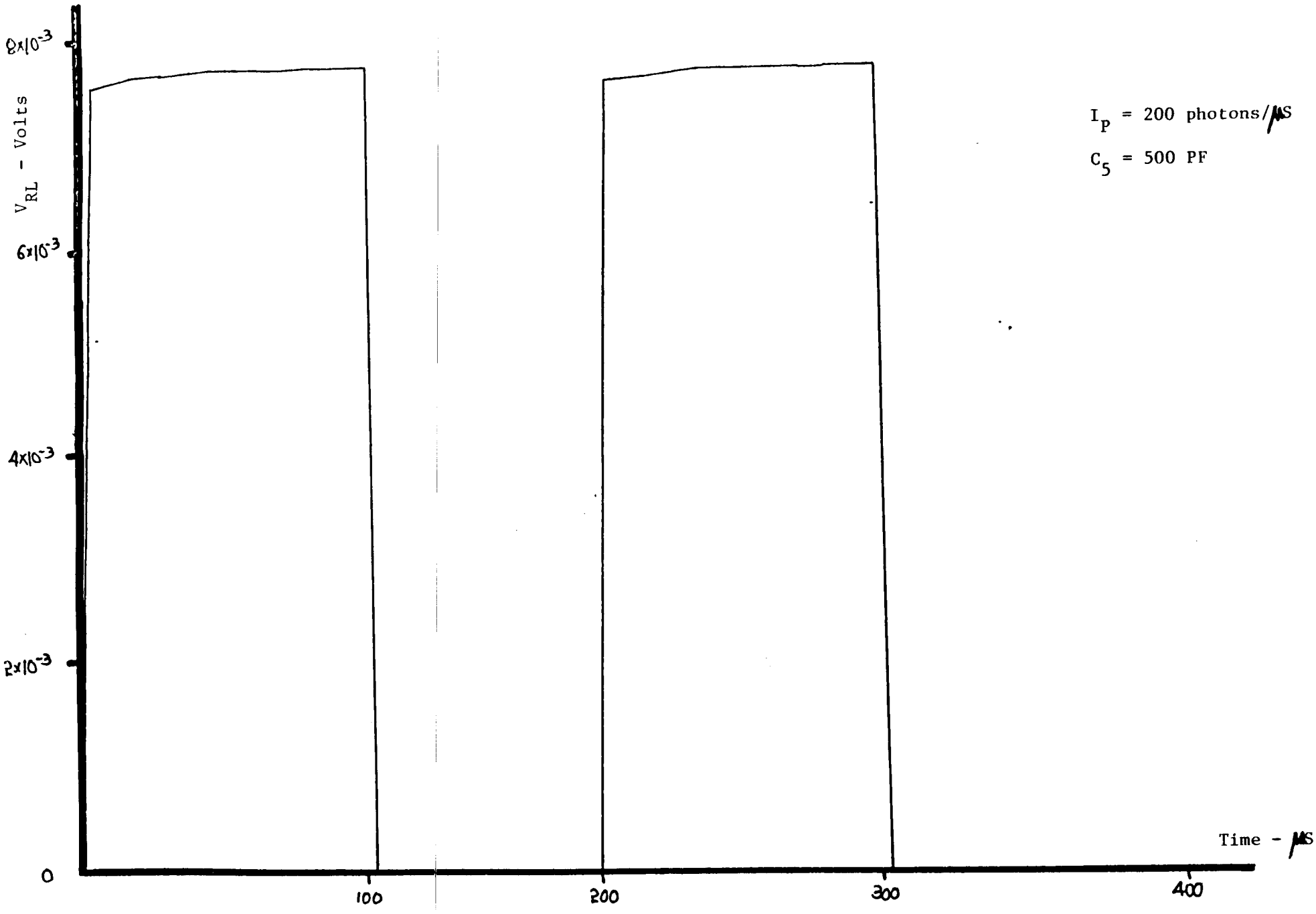

Figure 18 - Output Voltage Across R_L

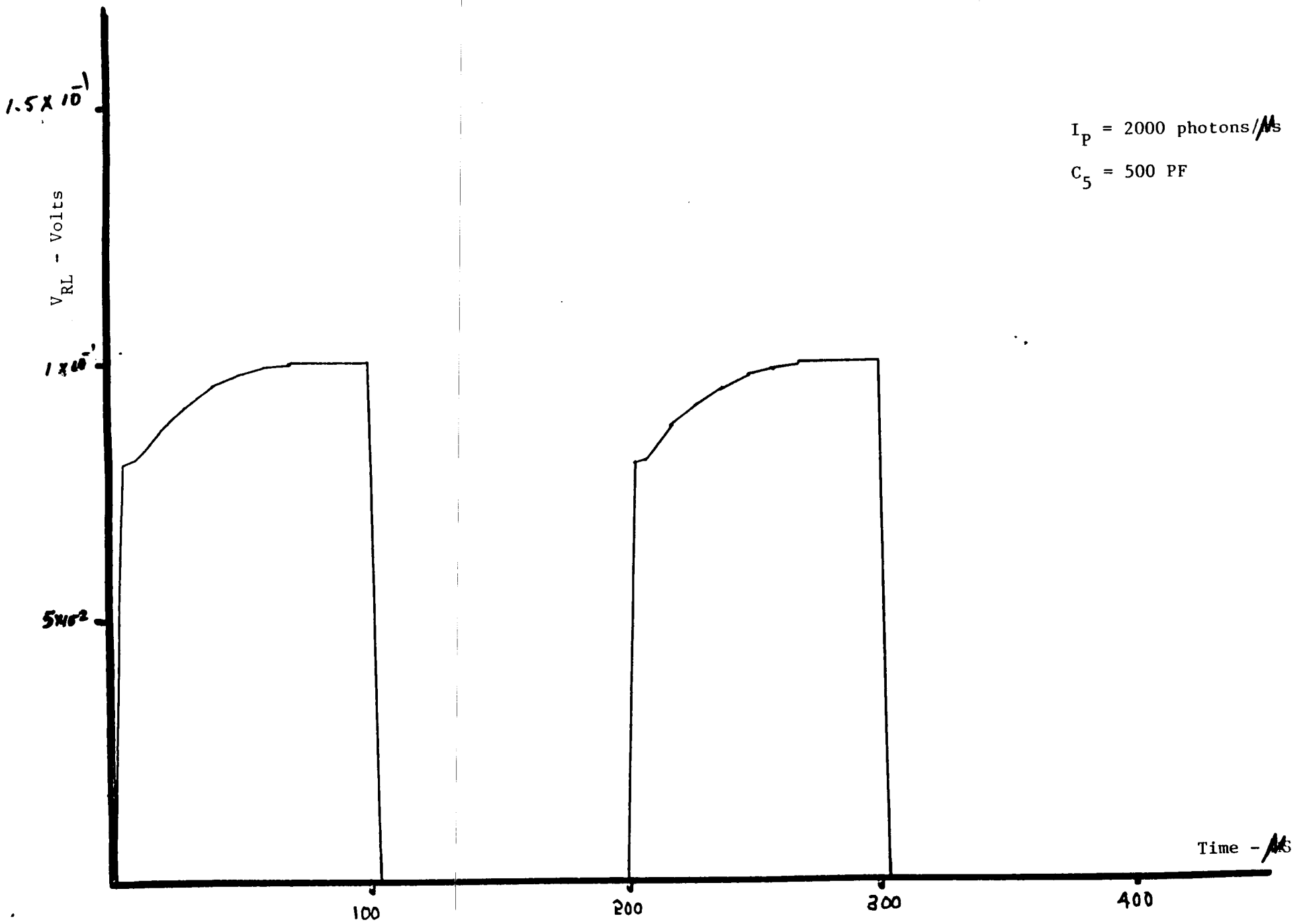

Figure 18 - Output Voltage Across R_L

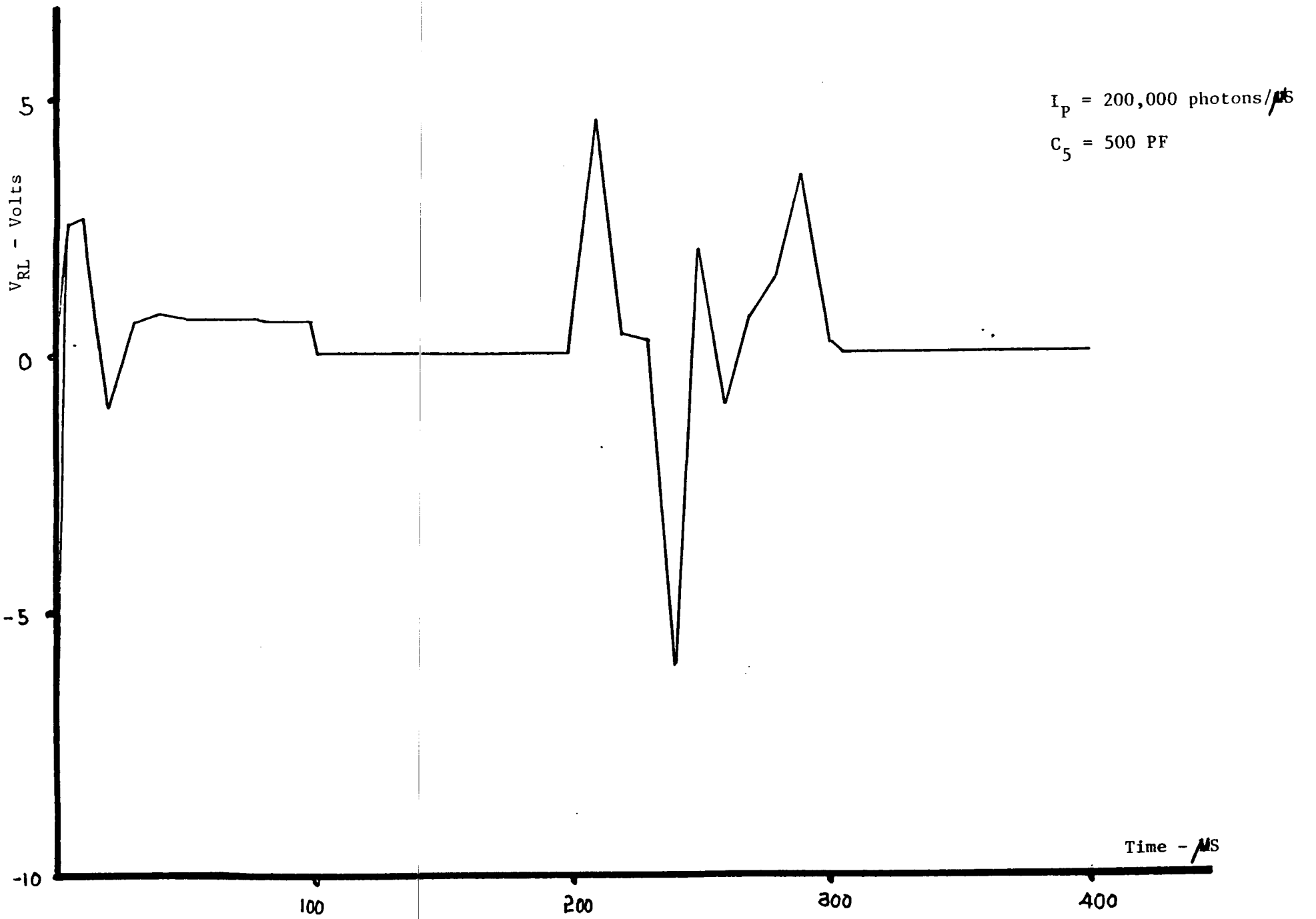

Figure 19 - Output Voltage Across R_L

PART II

UV DIAL MEASUREMENTS OF O_3 PROFILES IN REGIONS OF SPATIALLY INHOMOGENEOUS AEROSOLS

BY

S. R. YOO AND R. H. LANG

ABSTRACT

In the DIAL measurement of the O_3 concentration profile the corrections due to aerosol backscattering and interference in two wide gap wavelengths are discussed in regions of spatially inhomogeneous aerosols. A new Bernoulli solution for determining the relative distribution of aerosol backscattering is presented, and the boundary values for these solutions are discussed. For the multiple scattering effect, a factor is added in a new Bernoulli solution. It is shown that this factor results in a small correction in O_3 concentration profile.

CONTENTS

UV DIAL Measurements of O_3 Profiles in Regions of Spatially Inhomogeneous Aerosols

I. Introduction

With the advent of Lidar systems, great advances have been made in recent years in the remote sensing of the atmosphere. The Differential Absorption Lidar (DIAL) technique, using the Lidar system, has been used to obtain vertical profiles of atmospheric gas concentrations from ground, and airborne platforms. The major advantage of the DIAL technique is that the result is independent of many system parameters.

This report represents a continuation of the work which has been done by Browell, Ismail, and Shiply in the NASA research center.[1] They have presented the new Bernoulli solution for inverting lidar returns in the UV DIAL O_3 measurement. In this report we reproduce and improve a part of the results of the new solution, and discuss the multiple scattering effects on the lidar returns. A brief summary of the new Bernoulli solution in the UV DIAL O_3 measurements presented by Browell, et. al, is as follows.

By using the DIAL technique the atmospheric gas concentrations as a function of range can be found. The measurements involve two types of errors, called backscattering error and extinction error. The backscattering error is due to interference by aerosol backsca-

ttering, and the extinction error is due to difference between Rayleigh and aerosol volume extinction coefficients at the on and off wavelengths, respectively. Because of the wide gap of the on and the off wavelengths in the UV DIAL O_3 measurements, these error terms can not be ignored. By using the wavelength dependency of scattering coefficients, the extiction error is found in terms of the scattering coefficients at the off wavelength, and the difference of the absorption cross-section at the on and the off wavelengths. Assuming a power relationship between the backscattering coefficient and the total scattering coefficient(i.e., power law), the backscattering error is expressed in terms of the backscattering ratio at the off wavelength, which is the ratio of the aerosol to the Rayleigh volume backscattering coefficients. To calculate the backscattering error, the backscattering ratio should be obtained. In case of aerosol dominated atmospheric scattering, the distribution of aerosol volume backscattering along the lidar path can be found by solving the Bernoulli equation for the lidar returns. Since the Rayleigh component of scattering near UV wavelength has as much importance as the aerosol component, the new Bernoulli equation including the Rayleigh and aerosol terms has been derived and solved. The quantitative analysis of two correction terms shows that the extinction error of Rayleigh is found to be 6.7 ppb (independent of altitude) and the backscatter correction ranges from - 8 ppb to 22 ppb. However, the extinction error of aerosol has not been implemented in the DIAL data reduction because of the uncertainties in the knowledge of aerosol extinction coefficient, and the aerosol extinction

correction has been remainded in the further works.

In this paper, we try to solve the problems which have been suggested for further work[1]. One is to estimate the aerosol backscattering coefficient at low altitude and to obtain the gas concentration of interest at lower altitude from this, and the other is to apply the aerosol extinction correction into the DIAL O_3 measurements. In other words, the number density of gas of interest can be found by estimating the exact boundary value of Bernoulli solution at R_m. Furthermore, multiple scattering effects are examined to improve the inversion of O_3 profile in the UV DIAL measurements.

In the next chapter, the single scattering measurements are briefly described and in the following chapter the multiple scattering is applied into the UV DIAL O_3 measurements. By examining the multiple scattering effects, a small reduction of the extinction correction is expected.

In the chapter IV, an algorithm for estimation of boundary value of the new Bernoulli solution is presented by a simple algebric calculation and the sensitivity of Bernoulli solution to the input parameters is discussed.

II. Single Scattering in the UV DIAL O_3 Measurements.

Ever since the lidar system was introduced in the early 1960's, algorithms for inverting lidar return signals have been discussed in the literatures.[3,4] Until recently, however, the inversion of lidar returns has been plagued by instability and inaccuracies. The instability of previous solutions is found to be caused by mathematical and not, as some have suggested, physical reasons. Inaccuracies can occur by making unnecessary assumptions to further simplify the equation. The solution proposed by Klett[8] in 1981 was a step to improve this situation.

A. Lidar Equation.

The lidar equation is the governing relation which permits the calculation of the extinction coefficient and estimates of concentration under conditions of single scattering from a given lidar return. The lidar equation can be derived from the radar equation, the equation of radiative transfer, or the equations related on the laser radiation. It is convenient to begin with the equation of radiative transfer since it reveals the physical assumptions made in the lidar equation:

$$\frac{dI_f(R,\underline{s})}{dR} = -\alpha_t(R)\cdot I_f(R,\underline{s}) + \frac{\alpha_t(R)}{4\pi}\int_{4\pi} P(\underline{s},\underline{s}')\cdot I_f(R,\underline{s})\cdot d\Omega' + \varepsilon(R,\underline{s})$$

$$= -\alpha(R)\cdot[I_f(R,\underline{s}) - J_f(R,\underline{s})] \qquad (1)$$

where $I_f(R,\underline{s})$ is the specific intensity of radiation at frequency f

in the $\underline{s}$ direction, $\alpha(R)$ is the total scattering and extinction coefficient, and $J_f(R,\underline{s})$ is the source term. The source term contains contribution to scattering from all $\underline{s}'$ direction and emission in the $\underline{s}$ direction, i.e., $\epsilon(R,\underline{s})$. $P(\underline{s},\underline{s}')$ is the scattering phase function. In the radiative transfer equation, an important assumption has already been made: that the distance between the scatterers is larger than the wavelength, and the scattered radiation is incoherent and interference effects are not considered.

For the next step in deriving the lidar equation, the assumption is made that $I_f(R,\underline{s}) >> J_f(R,\underline{s})$. This assumes that there are no significant amount of emission or scattering from the medium in the direction of propagation. Note that this contains the critical assumption that only single scattering events occur. In making this assumption we obtain

$$\frac{1}{I_f}\frac{dI_f(R)}{dR} = -\alpha_t(R) \tag{2}$$

or

$$I_f(R) = I_o \exp\{-\int \alpha_t(r')dr'\} \tag{3}$$

with I_o being the initial intensity of the beam before any extinction. We note that the equation (2) is a function of range only and equation (3) is the well-known Beer's law.

For the lidar system in which the return power is being received in the direction opposite to the beam direction, the return power will be proportional to the initial transmitted power P_o, geometric attenuation A/R^2, where A is the receiver area, and the folded laser

pulse length given by $c\tau/2$, where c is speed of light and τ is the time duration of the laser pulse. Furthermore, the return power will depend on the volume backscattering coefficient, $\beta_\pi(R)$, at range R, and finally on a system function F(R) which includes parameters such as system sensitivity and geometric crossover of the receiver and laser beam. Putting all these factors together with equation (3), we obtain the lidar equation:

$$P(R) = P_o \frac{c\tau}{2} F(R)\cdot\beta_\pi(R) \frac{A}{R^2} \exp\{ -2\int_o^R \alpha(r)\, dr\} \qquad (4)$$

where the extinction term in Beer's law has been squared since the return power must traverse the same medium twice.

As we discussed above, the assumptions in the lidar equation (4) can be summarized as followings:

1. incoherent scatterers (Equation of radiative transfer),
2. single scattering, $I_f >> J_f$,
3. only backscattering is considered, $\beta_\pi(R)$,
4. Monochromatic ligt source.
5. Beam overlay is complete, i.e., no blind spot.

B. Differential Absorption Lidar (DIAL) Technique.

Differential Absorption Lidar is a single ended active remote sensing technique for monitoring concentration of various atmospheric gases. In the DIAL technique two laser pulses of slightly different wavelength, where one is chosen to coincide with a strong absorption feature of the specific constituent of interest and the other lies in the wing of this feature, are used and the attenuation of the two pulses is compared. The wavelengths of two pulses will be called the on and off wavelengths in this paper.

For a monostatic single-frequency pulsed lidar, the single scattering lidar equation is obtained in equation (4). The ratio of the return power signals at the on and off wavelengths, i.e., $P(\lambda_{on},R)$ and $P(\lambda_{off},R)$, respectively, is expressed in this form:

$$\frac{P(\lambda_{on},R)}{P(\lambda_{off},R)} = \frac{\beta_\pi(\lambda_{on},R)}{\beta_\pi(\lambda_{off},R)} \exp\left[-2\int_o^R \{\alpha(\lambda_{on},r) - \alpha(\lambda_{off},r)\}dr\right] \qquad (5)$$

where the subscripts of on and off refer to the on and off wavelengths. In equation (5) we assume that the all system parameters at both wavelengths are equal:

$$F(\lambda_{on},R) = F(\lambda_{off},R). \qquad (6)$$

The total volume extinction coefficient, $\alpha(\lambda,r)$, is composed of scattering terms and absorption terms of atmospheric components (e.g., gases and aerosols). Hence:

$$\alpha(\lambda,R) = \alpha_s(\lambda,R) + \alpha_a(\lambda,R). \qquad (7)$$

In the DIAL technique, the absorption of the lidar power is

mainly caused by the gases of interest. The total volume extinction coefficient of absorption, then, is the sum of the extinction coefficient of absorption due to each gases;

$$\alpha_a(\lambda,R) = \sum_i^n \alpha_a^i(\lambda,R) = N(R)\cdot\sigma_a(\lambda) \tag{8}$$

where N(R) represents the number density of the gas of interest which causes the absorption, and σ_a is its absorption cross section. Substituting equations (7) and (8) into (5), and taking log and integral yield:

$$\int_o^R N(r)\cdot\Delta\sigma_a\cdot dr = \frac{1}{2}\ln\frac{P(\lambda_{off},R)}{P(\lambda_{on},R)} - \frac{1}{2}\ln\frac{\beta_\pi(\lambda_{off},R)}{\beta_\pi(\lambda_{on},R)}$$

$$- \int_o^R \{\alpha_s(\lambda_{on},r) - \alpha_s(\lambda_{off},r)\}dr \tag{9}$$

where we have introduced the differential absorption cross section, $\Delta\sigma_a$, that is the difference of the absorption cross section at the <u>on</u> and <u>off</u> wavelengths:

$$\Delta\sigma_a = \sigma_a(\lambda_{on}) - \sigma_a(\lambda_{off}) \tag{10}$$

If we define the average number density of gas and assume that the volume scattering coefficient $\alpha_s(r)$ is constant over the range increment (interval), $\Delta R = R_2 - R_1$, i.e.,

$$N_{R_1,R_2} \approx \frac{1}{\Delta R}\int_{R_1}^{R_2} N(r)\cdot dr \tag{11}$$

and

$$\alpha_s(\lambda)_{R_1,R_2} \approx \frac{1}{\Delta R}\int_{R_1}^{R_2}\alpha_s(\lambda,r) = \frac{\tau_e(\lambda)}{\Delta R} \tag{12}$$

where τ_e represents the differential extinction spatial depth for the atmosphere.

From the assumption of (11) and (12), the range information of the gas of interest can be obtained in the interval, R_1 and R_2:

$$N_{R_1,R_2} = \frac{1}{2\Delta R\cdot\Delta\sigma_a}\ln\frac{P(\lambda_{on},R_1)}{P(\lambda_{on},R_2)}\cdot\frac{P(\lambda_{off},R_2)}{P(\lambda_{off},R_1)} \quad \{M\}$$

$$- \frac{1}{2\Delta R\cdot\Delta\sigma_a}\ln\frac{\beta_\pi(\lambda_{on},R_1)}{\beta_\pi(\lambda_{on},R_2)}\cdot\frac{\beta_\pi(\lambda_{off},R_1)}{\beta_\pi(\lambda_{off},R_2)} \quad \{B\}$$

$$- \frac{1}{2\Delta\sigma_a}\{\alpha_s(\lambda_{on}) - \alpha_s(\lambda_{off})\}_{R_1,R_2} \quad \{E\} \tag{13}$$

For the O_3 number density in the DIAL measurements, we rewrite equation (13) in this form:

$$N(O_3)_{R_1,R_2} = \{MO_3\} + \{BO_3\} + \{EO_3\} \tag{14}$$

The terms $\{BO_3\}$ and $\{EO_3\}$ in equation (13) are the corrections to the DIAL measurements due to the wavelength dependence of back-scattering and volume scattering of atmospheric gases. Under conditions of spatially homogeneous atmosphere the term $\{BO_3\}$ can be neglected, i.e., since $\beta_\pi(R_1) = \beta_\pi(R_2)$. Also, when the on and off

wavelengths are close together, the term $\{EO_3\}$ generally becomes negligible. Then only term $\{MO_3\}$ can be used to evaluate the range concentration in the DIAL measurements.

In the UV DIAL measurements for the density of O_3, neither of these conditions are present under normal atmospheric circumstances because ozone is usually distributed inhomogeneously in the normal atmosphere and the wide gap between wavelengths for the on and off frequencies are used in the O_3 measurement (286 nm and 298.3 nm). The error terms, i.e., $\{BO_3\}$ and $\{EO_3\}$, will be regarded to as the backscatter error and the extinction error, respectively. These two terms for the O_3 measurement will be discussed in the next section.

C. Two Interference Terms in the O_3 Measurements.

In most common scattering situations, separation of the gaseous (Rayleigh scattering) and aerosol (Mie scattering) components from the lidar measurements is needed. The volume backscattering coefficient and the volume extinction coefficient due to scattering can be expressed in the sum of their coefficients of the gaseous and aerosol components:

$$\beta_{\pi}(\lambda,R) = \beta_{\pi,R}(\lambda,R) + \beta_{\pi,M}(\lambda,R)$$
$$\alpha_{s}(\lambda,R) = \alpha_{s,R}(\lambda,R) + \alpha_{s,M}(\lambda,R) \qquad (15)$$

where subscripts R and M represent the gaseous (Rayleigh scattering) and aerosol (Mie scattering) components, respectively.

The volume scattering coefficients for gaseous and molecular components are dependent on the wavelength. These coefficients vary inversely with wavelength as powers, 4 and δ, respectively(Collis and Russell[4]):

$$\alpha_{s,R}(\lambda) \approx \alpha_{s,R}\cdot\lambda^{-4}$$
$$\alpha_{s,M}(\lambda) \approx \alpha_{s,M}\cdot\lambda^{-\delta} \qquad (16)$$

where $\alpha_{s,R}$ and $\alpha_{s,M}$ are the average scattering coefficients independent of wavelength in range R_1 and R_2.

Using Taylor expansion, i.e., $f(x) \approx f(x_o) + f'(x_o)(x - x_o)$, we can write the volume scattering coefficient at the on wavelength by:

$$\alpha_{s}(\lambda_{on}) \approx \alpha_{s}(\lambda_{off}) + \alpha'_{s}(\lambda_{off})\cdot(\lambda_{on} - \lambda_{off}) \qquad (17)$$

or defining that $\Delta\lambda = \lambda_{on} - \lambda_{off}$, we find:

$$\alpha_s(\lambda_{on}) - \alpha_s(\lambda_{off}) \approx \alpha'_s(\lambda_{off}) \cdot$$

$$= \frac{\Delta\lambda}{\lambda_{off}} \{4 \cdot \alpha_R(\lambda_{off}) + \delta \cdot \alpha_M(\lambda_{off})\}. \qquad (18)$$

Therefore, the extinction error $\{EO_3\}$ in interval range R_1 and R_2 in equation (14) can be approximated in this form:

$$\{EO_3\}_{R_1,R_2} \approx \frac{1}{\sigma_a} \frac{\Delta\lambda}{\lambda_{off}} \{ 4 \cdot \alpha_{s,R}(\lambda_{off}) + \delta \cdot \alpha_{s,M}(\lambda_{off}) \}. \qquad (19)$$

The scattering coefficients at the off wavelength do not cause absorption. These coefficients can be obtained from the relation:

$$\alpha_{s,R}(\lambda,R) \approx N_R(R) \cdot \sigma_{s,R}(\lambda) \cdot$$

$$\alpha_{s,M}(\lambda,R) \approx N_M(R) \cdot \sigma_{s,M}(\lambda) \cdot \qquad (20)$$

where $N_R(R)$ and $N_M(R)$ represent the number density of gases(Rayleigh) and aerosols, and $\sigma_{s,R}(\lambda)$ and $\sigma_{s,M}(\lambda)$ are their cross section.

Typically the Rayleigh number density can be taken from the U.S. standard atmospheric number density.

The backscattering correction $\{BO_3\}$ can be evaluated by introducing the backscatter ratio that is the ratio of the backscattering coefficients for gaseous and molecular components:

$$b_\lambda(R) = \frac{\beta_{\pi,M}(\lambda,R)}{\beta_{\pi,R}(\lambda,R)} \qquad (21)$$

In equation (21), the relation of volume backscattering coefficient and volume extinction coefficient due to scattering is needed to further simplify the backscatter ratio. The traditional way to account for any dependence between the β_π and α_s is to assume a power relationship of this form:

$$\beta_\pi(\lambda,R) = B_o \cdot \alpha_s^k(\lambda,R) \tag{22}$$

where k depends on the lidar wavelength and various properties of the obscuring aerosol, and B_o is constant. Klett[8] has indicated that the value of the exponent k is generally in the range $0.67 \le k \le 1.0$. Although k is no longer unity, the ratio of backscattering to extinction coefficients, B_o, can be found by assuming that $k = 1$ in absence of absorption. We will consider later the case of $k = 1$. The backscattering/extinction ratios for Rayleigh to aerosols components in general have been expressed in the form:

$$\begin{aligned} \beta_{\pi,R}(\lambda,R) &= \frac{3}{8\pi}\cdot\alpha_{s,R}(\lambda,R) \\ \beta_{\pi,M}(\lambda,R) &= \bar{P}_\pi\cdot\alpha_{s,M}(\lambda,R) \end{aligned} \tag{23}$$

where $\bar{P}_\pi = P_\pi/4\pi$ is the normal aerosol backscattering phase function and is taken to be a constant for the isotropic scattering.

Noting the wavelength dependence in the extinction coefficients ,i.e., Eq.(16), the backscatter ratio can be expressed in the form:[11]

$$b_\lambda(R) \approx \frac{\bar{P}_\pi\cdot\alpha_{s,M}(R)\cdot\lambda^{-\delta}}{3/8\pi\cdot\alpha_{s,R}(R)\cdot\lambda^{-4}} = b_o(R)\cdot\lambda^{4-\delta} \tag{24}$$

The backscatter ratio at the on wavelength in terms of that at the off wavelength becomes:

$$b_{on}(R) = b_{off}(R)\cdot\left(\frac{\lambda_{on}}{\lambda_{off}}\right)^{4-\delta}$$

$$= b_{off}(R)\cdot\left(1 - \frac{\Delta\lambda}{\lambda_{off}}\right)^{4-\delta} \qquad (25)$$

Knowing that $\Delta\lambda = \lambda_{off} - \lambda_{on}$ is small, we have:

$$b_{on}(R) \approx b_{off}(R)\cdot\left\{1 - (4-\delta)\cdot\frac{\Delta\lambda}{\lambda_{off}}\right\} \qquad (26)$$

or

$$b_{on}(R) - b_{off}(R) \approx (4-\delta)\cdot\frac{\Delta\lambda}{\lambda_{off}}\cdot b_{off}(R) \qquad (27)$$

To obtain the $\{BO_3\}$ in terms of the backscatter ratio, we consider that:

$$\frac{\beta_\pi(\lambda_{on},R)}{\beta_\pi(\lambda_{off},R)} = \frac{\beta_R(\lambda_{on},R)}{\beta_R(\lambda_{off},R)}\cdot\left\{\frac{1 + b_{on}(R)}{1 + b_{off}(R)}\right\}$$

$$= \left(\frac{\lambda_{on}}{\lambda_{off}}\right)^{4}\cdot\left\{1 + \frac{b_{on}(R) - b_{off}(R)}{1 + b_{off}(R)}\right\} \qquad (28)$$

where the wavelength dependence in the backscattering coefficient of Rayleigh component at the on and off wavelength has been assumed.

By substituting (27) into (28) and taking logarithm, we have:

$$\ln\left(1 - 4\cdot\frac{\Delta\lambda}{\lambda_{off}}\right) + \ln\left(1 - \frac{(4-\delta)\cdot\Delta\lambda}{\lambda_{off}}\cdot\frac{b_{off}(R)}{1 + b_{off}(R)}\right)$$

$$\approx -4\cdot\frac{\Delta\lambda}{\lambda off} - \frac{(4-\delta)\cdot\Delta\lambda}{\lambda\, off}\cdot\frac{b_{off}(R)}{1+b_{off}(R)} \qquad (29)$$

where the approximation in equation (29) has been made, i.e., $\log(1+x) \approx x$, as $x \ll 1$.

Finally, the backscatter correction $\{BO_3\}$ in interval range R_1 and R_2 in equation (14) is obtained in the form:

$$\{BO_3\} \approx \frac{(4-\delta)}{2\cdot R\cdot \sigma_a}\cdot\frac{\Delta\lambda}{\lambda_{off}}\cdot\left\{\frac{b_{off}(R_2)}{1+b_{off}(R_2)} - \frac{b_{off}(R_1)}{1+b_{off}(R_1)}\right\} \qquad (30)$$

To calculate the $\{BO_3\}$, we need to evaluate the backscatter ratio at the off wavelength. In other words, the aerosol backscattering profile along the lidar return path must be obtained. From equations (21) and (23), we can rewrite the backscatter ratio in terms of the function $g_\lambda(R)$ by:

$$b_\lambda(R) = \frac{\alpha_{s,M}(\lambda,R)}{g_\lambda(R)} \qquad (31)$$

where the function g (R) is represented by:

$$g_\lambda(R) = \frac{3/8\pi\cdot\alpha_{s,R}(\lambda,R)}{\bar{P}_\pi(R)} \qquad (32)$$

Since the Rayleigh scattering coefficient can be obtained in the relation in equation (20), $g_\lambda(R)$ is a known function. As mentioned above, the aerosol distribution profile along the lidar path needs to be found. It can be obtained by solving the Bernoulli equation which contains the Rayleigh and the aerosol scattering components.

D. Inversion Methods and New Bernoulli Solution for the UV DIAL O_3 Measurements.

From the single scattering lidar equation, the inversion of extinction coefficients has been discussed in the slope and ratio method, Bernoulli method(forward or backward inversion methods), AGIL method[5], etc. In these methods, the basic relation of equation (22) has been assumed. Noting that the following definition is made:

$$S(R) = \ln[R^2 \cdot P(R)] \tag{33}$$

we can derive the differential equation for the extinction coefficient:

$$\frac{dS}{dR} = \frac{k}{\alpha} \cdot \frac{d\alpha}{dR} - 2\alpha \tag{34}$$

In deriving equation (34), the system parameter F(R) and B_o are assumed to be constants.

The following sections briefly review the major inversion methods and the new Bernoulli solution for the UV DIAL O_3 measurements.

1. Inversion Method of the Lidar Equation.

The brief review of inversion of Lidar return signals is summarized in the followings:

Slope and Ratio method

If one assumes that over some distance the aerosol is uniform, i.e., $d\alpha/dR = 0.$, we can have:

$$\alpha = -\frac{1}{2}\cdot\frac{dS}{dR} \tag{35}$$

so that the slope of a plot of S versus R will give us the value of α over the homogeneous region. This can be however a very poor approximation if there is noise or if the medium is inhomogeneous. The ratio method is just a variant of the slope method when it is applied segment by segment. Note that the equation would result from the assumption that $k = 0$, i.e., the backscattering is a constant independent of the aerosol concentration. The slope method has been used most often in the past since it is simple.

Bernoulli method.

The equation (34) can be solved exactly because it is a standard differential equation, namely the Bernoulli equation or a homogeneous Ricatti equation. The solution, which is called the forward integral method, is:

$$\alpha(R) = \frac{\exp[(S - S_o)/k]}{\{\alpha_o^{-1} - \frac{2}{k}\cdot\int_{R_o}^{R}\exp[(S - S_o)/k]dr\}} \tag{36}$$

where the subscript o refers to the reference distance R_o which is the closest to the lidar system. This solution is however unstable since two relatively large terms are subtracted in the denominator to obtain a small difference(Klett, 1981)[9]. Thus, if there is an error in α_m, the solution quickly becomes unstable, and an unrealistic

value of $\alpha(R)$ are computed at modestly small R. In order to obtain the stable solution of $\alpha(R)$, the idea of making a guess or measurement of $\alpha(R)$ at the largest distance from the lidar system, i.e., α_m, was mentioned in the reference. However, after some unsuccessful attempts, Klett obtained the following solution which is called the backward integral method:[8]

$$\alpha(R) = \frac{\exp[(S - S_m)/k]}{\{\alpha_m^{-1} + \frac{2}{k}\int_R^{R_m} \exp[(S - S_m)/k]dr\}} \tag{37}$$

where the subscript m refers to the reference distance R_m which is the furthest from the lidar system. Now that the two expressions were added in the denominator, the solution becomes more stable. Furthermore, the error in α_m becomes less important as R decreases and the integral in (37) increases. Thus the solution will tend to converge to the correct $\alpha(R)$ as R gets smaller. However, the boundary value α_m must still be determined.

2. New Bernoulli Solution in the UV DIAL O_3 Measurements.

In order to construct an Bernoulli equation in the DIAL technique we define the normal lidar return in the form:

$$\mu_\lambda(R) = \frac{P(\lambda,R)\cdot R^2}{P(\lambda,R_o)\cdot R_o^2} \tag{38}$$

where the subscript o refers to the reference distance R_o which is the closest to the lidar system.

Recalling the lidar equation (4) and the relations of the

$$\mu_\lambda(R) = \frac{\beta_\pi(\lambda,R)}{\beta_\pi(\lambda,R_o)} \cdot \exp\{-2\int_{R_o}^{R}[\alpha_s(\lambda,r) + N(r)\cdot\sigma_a(\lambda)]dr\} \qquad (39)$$

The ratio of the backscattering coefficients in range R and R_o can be written in terms of the backscatter ratio defined in (21):

$$\frac{\beta_\pi(\lambda,R)}{\beta_\pi(\lambda,R_o)} = \frac{\beta_{\pi,R}(\lambda,R)}{\beta_{\pi,R}(\lambda,R_o)} \cdot \{\frac{1 + b_\lambda(R)}{1 + b_\lambda(R_o)}\} \qquad (40)$$

By defining that the scatter ratio is:

$$\Phi_\lambda(R) = \frac{\beta_\pi(\lambda,R)}{\beta_{\pi,R}(\lambda,R)} = 1 + b_\lambda(R) \qquad (41)$$

and from equations (15) and (20), we find:

$$\mu_\lambda(R) = \frac{N_R(R)}{N_R(R_o)} \cdot \frac{\Phi_\lambda(R)}{\Phi_\lambda(R_o)} \cdot \exp\{-2\int_{R_o}^{R}[\alpha_{s,R}(\lambda,r) + \alpha_{s,M}(\lambda,r) + N(r)\cdot\sigma_a(\lambda)]dr\} \qquad (42)$$

where $N_R(R)$ and $N(R)$ refer to the Rayleigh gas number density and the gas number density absorbing the lidar power, respectively.

Since the Rayleigh component of scattering near UV wavelength has as much importance as the aerosol component, the extinction coefficient due to Rayleigh component is specified in equation (42). Let $\mu_\lambda^*(R)$ represent the normalized lidar return corrected for Rayleigh scattering and absorption such that:

$$\mu_\lambda^*(R) = \mu_\lambda(R) \frac{N_R(R_o)}{N_R(R)} \cdot \exp\{+2\int_{R_o}^{R}[\alpha_{s,R}(\lambda,r) + N(r)\cdot\sigma_a(\lambda)]dr\} \qquad (43)$$

Substituting (43) into (42), we get:

$$\mu_\lambda^*(R) = \frac{\Phi_\lambda(R)}{\Phi_\lambda(R_o)} \cdot \exp\{ -2 \int_{R_o}^{R} \alpha_{s,M}(\lambda, r) \cdot dr \} \tag{44}$$

where the absorption term in (42) and (43) can be neglected at the off wavelength. The extinction coefficient due to the aerosol scattering, $\alpha_{s,M}(\lambda,R)$ can be written in the expression:

$$\alpha_{s,M}(\lambda, R) = g_\lambda(R) \cdot b_\lambda(R) = g_\lambda(R) \cdot [\Phi_\lambda(R) - 1] \tag{45}$$

where $g_\lambda(r)$ and $b_\lambda(r)$ have been defined in the equations (21) and (32). Then taking log, differentiating, and rearranging the equation (44), we have the form of a differential equation:

$$\frac{d\Phi}{dR} = \Phi(R)\{ \frac{d}{dR} \ln \mu_\lambda^*(R) - 2 \cdot g(R) \} + 2 \cdot g(R) \cdot \Phi^2(R) \tag{46}$$

This is the inhomogeneous linear equation of Bernoulli equation:

$$y' = a(x) \cdot y + b(r) \cdot y^2 \tag{47}$$

with the solution:

$$y = \frac{C_1}{I(x)} - \frac{1}{I(x)} \int^{x} b(t) \cdot I(t) \cdot dt \tag{48}$$

where

$$I(x) = \exp(\int^{x} a(t) \cdot dt) \tag{49}$$

Following the steps above, we have found the solution of the

Following the steps above, we have found the solution of the equation (46):

$$\Phi_\lambda(R) = \frac{\mu^*_\lambda(R)\cdot\exp[-2\int_{R_o}^{R} g(r)dr]}{\Phi_o^{-1} - 2\cdot\int_{R_o}^{R} dr\ [g(r)\cdot\mu^*_\lambda(r)\cdot\exp\{-2\int_{R_o}^{r} g(r')\cdot dr'\}]} \qquad (50)$$

where $\mu^*_\lambda(R_o) = 1.$, and Φ_o is the boundary value at range R_o which is the nearest to the lidar system.

Using the idea of the backward integration method, we can obtain the stable solution of the equation (46) in the expression:

$$\Phi_\lambda(R) = \frac{\mu^*_\lambda(R)\cdot\exp[-2\int_{R}^{R_m} g(r)dr]}{\Phi_m^{-1} + 2\cdot\int_{R}^{R_m} dr[g(r)\cdot\mu^*_\lambda(r)\cdot\exp\{-2\int_{r}^{R_m} g(r')\cdot dr'\}]} \qquad (51)$$

where Φ_m is the boundary value at range R_m which is the furthest to the lidar system.

III. Multiple Scattering In the UV DIAL O_3 Measurements

In the previous chapter, the single scattering effect was considered in the inversion of the lidar equation. In this chapter, we discuss the multiple scattering effects on the lidar equation and the UV DIAL O_3 measurements.

A. Multiple Scattering corrections in the Lidar Equation and the UV DIAL O_3 Measurements.

As mentioned earlier, the multiple scattering effects have been considered in the inhomogenious or dense media such as cloud, fog and rain falls. When the cloud is dense enough, significant multiple scattering will invalidate the lidar equation. Thus, either a new lidar equation incorporating multiple scattering should be used or the data adjusted so that only the single scattering component of the signal is considered.

In the earlier papers,[14,15] a simple expression of lidar equation with multiple scattering factor has been obtained in the form:

$$P(R) = P_o \cdot \frac{c\tau}{2} \cdot F(R) \cdot \beta_\pi(R) \cdot \frac{A}{R^2} \cdot \exp\{ -2 \int_{R_o}^{R} [\alpha(r) \cdot (1 - \Gamma(r))] dr \} \qquad (52)$$

where we note that the multiple scattering effect, $\Gamma(r)$ is taken into account inside the exponential term.

By examination of the available theories and experiments,[14,15] equation (52) would be considered when the optical depth is greater than 0.1 for lidar systems approximately 1 km or more from the media

and perhaps for optical depths greater than 1.0 when the lidar system distance is close (about 50 - 100 m). If the contribution of multiple scattering is small, the multiple scattering factor can be taken to be small and a constant.

In the DIAL technique, we can break the extinction coefficients into two terms due to scattering and absorption. Since the multiple scattering does not dominate the absorption, equation (52) can be written in the expression:

$$P(R) = P_o \cdot \frac{c\tau}{2} \cdot F(R) \cdot \beta_\pi(R) \cdot \frac{A}{R^2} \cdot \exp\{-2 \int_{R_o}^{R} [\alpha_s(r) \cdot (1 - \Gamma(r)) + \alpha_a(r)] dr\} \quad (53)$$

Assuming that the multiple scattering factor is small and a constant, and from the equation (8), we can write the equation (13) in the form :

$$\begin{aligned} N_{R_1,R_2} = & \frac{1}{2 \cdot \Delta R \cdot \Delta\sigma_a} \ln \frac{P(\lambda_{on},R_1)}{P(\lambda_{off},R_1)} \cdot \frac{P(\lambda_{off},R_2)}{P(\lambda_{on},R_2)} \\ & - \frac{1}{2 \cdot \Delta R \cdot \Delta\sigma_a} \ln \frac{\beta_\pi(\lambda_{on},R_1)}{\beta_\pi(\lambda_{off},R_1)} \cdot \frac{\beta_\pi(\lambda_{off},R_2)}{\beta_\pi(\lambda_{on},R_2)} \\ & - \frac{1}{\Delta\sigma_a} \cdot (1 - \Gamma) \cdot \{\alpha_s(\lambda_{on}) - \alpha_s(\lambda_{off})\}_{R_1,R_2} \end{aligned} \quad (54)$$

B. Corrected Bernoulli Solution In the UV DIAL O_3 Measurements.

As defined earlier, the normalized lidar return, taking the multiple scattering efffects into account, becomes:

$$\bar{\mu}_\lambda(R) = \frac{\beta_\pi(\lambda,R)}{\beta_\pi(\lambda,R_o)} \cdot \exp\{-2\int_{R_o}^{R} [\alpha_s(\lambda,r)\cdot(1 - \Gamma) + N(r)\cdot\sigma_a(\lambda)]dr\} \quad (55)$$

From equation (42), and by neglecting the small contribution of multiple scattering in the Rayleigth component, equation (42) becomes

$$\bar{\mu}_\lambda(R) = \frac{N_R(R)}{N_R(R_o)} \cdot \frac{\Phi(R)}{\Phi(R_o)} \cdot \exp\{-2\int_{R_o}^{R} [\alpha_{s,M}(\lambda,r)\cdot(1 - \Gamma) + \alpha_{s,R}(\lambda,r) + N(r)\cdot\sigma_a(\lambda)]dr\} \quad (56)$$

where $N_R(R)$ and $N(R)$ refer to the Rayleigh gas number density and the gas number density absorbing the lidar power as defined earlier, respectively. $\Phi_\lambda(R)$ is the scattering ratio as in equation (41).

The normalized lidar return corrected for Rayleigh scattering and absorption is defined in equation (43):

$$\bar{\mu}^*_\lambda(R) = \bar{\mu}_\lambda(R) \cdot \frac{N_R(R)}{N_R(R_o)} \cdot \exp\{+2\int_{R_o}^{R} [\alpha_{s,R}(\lambda,r) + N(R)\cdot\sigma_a(\lambda)]dr\} \quad (57)$$

Substituting (57) into (56), we find:

$$\bar{\mu}^*_\lambda(R) = \frac{\Phi_\lambda(R)}{\Phi_\lambda(R_o)} \cdot \exp\{-2\int_{R_o}^{R} \alpha_{s,M}(\lambda,r)\cdot(1 - \Gamma)\cdot dr\} \quad (58)$$

Following the steps in equations from (45) to (50), we found the stable solution of the corrected Bernoulli equation in the expression:

$$\Phi_\lambda(R) = \frac{\bar{\mu}^*_\lambda(R)\cdot\exp[-2\int_R^{R_m} g_\lambda(r)\cdot dr]}{\{\Phi_m^{-1} + 2\cdot\int_R^{R_m} dr[g_\lambda(r)\cdot\bar{\mu}^*_\lambda(r)\cdot\exp\{-2\int_r^{R_m} g_\lambda(r')\cdot dr'\}]} \qquad (59)$$

where g(r) is defined in equation (32) with k = 1.

$$g_\lambda(R) = \frac{3/8\pi\cdot\alpha^k_{s,R}(\lambda,R)}{\bar{P}_\pi} \qquad (60)$$

where k can not be taken to be k = 1.

IV. Analysis of DIAL Data for the O_3 measurement of in the UV Wavelength

DIAL data for the O_3 measurement in the UV was obtained from the on-board LIDAR system on 7 Aug. 1980 (Figs.A,B). In order to invert the Lidar return signal for the O_3 profile the new Bernoulli equation was derived and solved in the preview chapter. The solution of the new Bernuolli equation, i.e., $\Phi_\lambda(R)= 1 + b_\lambda(R)$, is given in Eqs.(50) and (51). For the reasons of numerical stability, backward integration of the Bernuolli solution is preferred to integration in the forward direction. However, the boudary condition at range R_m,i.e., $\Phi_m = \Phi(R_m)$, is unkown. Recently several of papers which describ the algorithm for estimating the boundary condition of the Bernuolli solution has been published by Ferguson and Stephens,[6] and Mulders[13] The algorithms of Ferguson and Stephens solved this problem by iteration, and the algorithm of Mulders solved the problem by simple algebra. Now we find the boundary value at range R_m, Φ_m, for the new Bernoulli solution by simple calculation in the following section A. In addition, some comments are made concerning the new Bernoulli solution at the low altitude. In the section B, we discuss the sensitivity of parameters such as $\bar{P}_\pi$, k, and Φ_m in the section B.

A. Estimation of Φ_m, Boundary Value.

The new Bernoulli solution requiring backward integration from some range R_m to R has been found in the Eq.(51).

$$\Phi_\lambda(R) = \frac{\bar{\mu}_\lambda^*(R)\cdot\exp[-2\int_R^{R_m} g(r)\cdot dr]}{\{\Phi_m^{-1} + 2\cdot\int_R^{R_m}[g(r)\cdot\bar{\mu}_\lambda^*(r)\cdot\exp\{-2\int_r^{R_m} g(r')\cdot dr'\}]dr}$$

Note that the normalized lidar return and the corrected lidar return at the off wavelength has been defined in the forms,

$$\bar{\mu}_{off}(R) = \frac{P(R)\cdot R^2}{P(R_m)\cdot R_m^2} \qquad (61)$$

Neglecting the absorption term at the off wavelength, the normalized lidar return for Rayleigh scattering extinction becomes,

$$\bar{\mu}^*(R) = \bar{\mu}_{off}(R)\,\frac{N_R(R_m)}{N_R(R)}\cdot\exp\{+2\int_R^{R_m}\alpha_{s,R}(r)dr\} \qquad (62)$$

and

$$g_{off}(R) = \frac{3/8\pi\cdot\alpha_{s,R}(R)}{\bar{P}_\pi}$$

The Rayleigh scattering extinction coefficient at wavelength, λ, and altitude Z, is defined by

$$\alpha_{s,R}(\lambda,Z) = \rho_R(Z)\cdot\sigma_R(\lambda) \qquad (63)$$

where the total Rayleigh scattering cross section $\sigma_R(\lambda)$, and the particle number density of air $\rho_R(Z)$ are assumed to be(Measures, 1984)

$$\sigma_R(\lambda) = \frac{8\pi}{3} \cdot \sigma_\pi \times \{ \frac{6 + 3\delta_p}{6 - 7\delta_p} \} \qquad [cm^2 sr^1] \tag{64}$$

$$\sigma_\pi(\lambda) = 5.45 \times \{ \frac{550}{\lambda(nm)} \}^4 \times 10^{-28} \qquad [cm^2 sr^{-1}]$$

$$\rho_R(Z) = N \cdot \exp\{ -Z/9.5 \} \qquad [molecules\ cm^{-3}]$$

Assume that the depolarization ratio δ_p for air is taken to be 0.042 and the particle number density of sea level, N, is taken to be 2.55 x 10 [molecules cm] from the U.S. standard atmosphere. Then, the scattering extiction coefficient at <u>off</u> wavelength 298.3 nm and altitude Z, can be found in the expression,

$$\alpha_{s,R}(Z) = 0.1444567 \exp\{ -Z/9.5 \} \qquad [km^{-1} sr^{-1}] \tag{65}$$

Let Z_a distance of the Lidar system from the ground, and R distance from the Lidar system to the actual altitude to be measured. Then the actual altitude becomes $Z = Z_a - R$ or $R = Z_a - Z$. Inspecting and applying the above equations, we find the expression,

$$\Phi_{off}(Z) = \frac{\bar{\mu}(Z_a - Z) \cdot \exp\{\frac{Z - Z_m}{9.5}\} \cdot \exp[C_1 \cdot \{\exp\frac{-Z}{9.5} - \exp\frac{-Z_m}{9.5}\}]}{\Phi_m^{-1} + C_2 \cdot \int_Z^{Z_m} dz' \cdot \bar{\mu}(Z_a - z') \cdot \exp[C_1\{\exp\frac{-z'}{9.5} - \exp\frac{-Z_m}{9.5}\}]} \tag{66}$$

where the constants C1 and C2 , are obtained by

$$C_1 = 2.746773 \text{ X } \{ \frac{3/8\pi}{P_\pi} - 1 \}$$

$$C_2 = 0.2889134 \text{ X } \frac{3/8\pi}{P_\pi} \text{ X } \exp\{-Zm/9.5\} \qquad (67)$$

The solution of the new Bernoulli equation was defined in the form,

$$\Phi_{off}(Z) = \frac{\beta_\pi(\lambda_{off},Z)}{\beta_{\pi,R}(\lambda_{off},Z)} = 1 + b_{off}(Z) \qquad (68)$$

and the backscatter ratio at off wavelength was defined by

$$b_{off}(Z) = \frac{\beta_{\pi,M}(\lambda_{off},Z)}{\beta_{\pi,R}(\lambda_{off},Z)} = \frac{\alpha_{s,M}(\lambda_{off},Z)}{g_{off}(Z)}$$

The backscatter ratio at the highest altitude , Z_o,(i.e., over 2000 meter) is assumed to be zero and then we can express the Eq.(51) in the form;

$$\Phi_{off}(Zo) = \frac{\bar{\mu}(Z_a - Z_o)\cdot\exp\{\frac{Z_o-Z_m}{9.5}\}\cdot\exp[C_1\cdot\{\exp\frac{-Z_o}{9.5} - \exp\frac{-Z_m}{9.5}\}]}{\Phi_m^{-1} + C_2\cdot\int_{Z_o}^{Z_m} dz'\cdot\bar{\mu}(Z_a-z')\cdot\exp[C_1\{\exp\frac{-z'}{9.5} - \exp\frac{-Z_m}{9.5}\}]} \qquad (69)$$

where

$$\Phi_{off}(Z_o) = 1 \qquad \text{for } Z_o > 2000 \text{ meter}$$

Hence, the integral constant or the bountary constant, Φ_m, at altitude Z_m can be found in the expression;

$$\Phi_m^{-1} = \bar{\mu}(Z_a - Z_o)\cdot\exp\{\frac{Z_o - Z_m}{9.5}\}\cdot\exp[C_1\cdot\{\exp\frac{-Z_o}{9.5} - \exp\frac{-Z_m}{9.5}\}]$$

$$- C_2\cdot\int_{Z_o}^{Z_m} dz'\cdot\bar{\mu}(Z_a - z')\cdot\exp[C_1\{\exp\frac{-z'}{9.5} - \exp\frac{-Z_m}{9.5}\}] \qquad (71)$$

The Eq.(71) shows that one may obtain the correct Φ_m using scalar iteration for the small deviation of the backscattering ratio at the highest altitude Z_o. However, the results by the slope method indicate that $\Phi_{off}(Z_o)$ is near 1.0 and it makes sense physically at high altitude over 2000 meter. This boundary value Φ_m can now be used in the new Bernoulli solution requiring forward integral, i.e.,Eq.(50), for the lower altitude(i.e., $Z < Z_m$). This is accomplished by replacing z with Z_m and performing the required integration.

B. Sensitivity of the New Bernoulli Solution to Input Parameters.

In this section, we examine the sensitivity of the Bernoulli solution to input parameters from the data set, (Fig., A,B), provided by NASA, Langley Research Center. The $\Phi(z)$ is computed by using Eq. (69) where the boundary value, Φ_m, is determined in the equation (71). In the equation (71), the boundary value is found in the range from 1.5 to 2.8 depending on the lowest altitude. Since the data provided by NASA is not accurate in the lower altitude range, three values of Φ_m have been chosen in order to complete the calculation. They are Φ_m = 2.0, 2.4, 2.8. Figure C shows the profiles which have been obtained for each case of the above three choices of Φ_m. Figures D and E show that the backscattering correction varies from -20 ppm at 1000 meter to 40 ppm at 2000 meter. The extinction error also varies from 6 to 20 ppm. This result includes a multiple scattering factor of 0.2. The corrected 0_3 profile is shown in the figure F. Comparing the uncorrected 0_3 profile, it reduces the sharpness at 1500 meter.

Reference

1. E.V. Browell, S.Isimail, and S.T.Shiply, "Ultraviolet DIAL Measurements of O_3 Profiles in Regions of Spatially Inhomogeneous Aerosols," App. Opt, Vol.24,No.17, p.2827 (Sept.1986)

2. Yasuhiro Sasano, Edward V. Browell, and Syed Ismail, "Error Caused by Using a constant Extinction/Backscattering Ratio in the Lidar Solution," App. Opt.,Vol.24,No.22,p.3929(1985)

3. R.T.H. Collis and P.B. Russell, "Lidar Measurement of Particles and Gases by Elastic Backscattering and differential Absorption," Laser Monitoring of the Atmospere, New York: Spring-Verlag (1976)

4. P.B. Russell, T.J. Swissler, and M.P. McCormick, "Methodology for Error Analysis and Simulation of Lidar Aerosol Measurements," App. Opt., Vol.18, No.22, p.3783 (Nov. 1979)

5. B.T.N. Evans, "On the Inversion of the Lidar Equation," Technical Report, File:3621B-005, (Nov. 1984)

6. J.A. Ferguson and D.H. Stephens, "Algorithm for Inverting Lidar Returns," App. Opt., Vol.22, No.22, No.13, p.3673(1983)

7. M.Kerker, The scattering of Light and Other Electromagnetic Radiation, New York: Academic Press (1969)

8. J.D. Klett, "Stable Analytical Inversion Solution for Processing Lidar Returns," App. Opt., Vol.20, No.2, p.211(1981)

9. J.D. Klett, "Lidar Calibration and Extinction Coefficients," App. Opt., Vol.22, No.4, p.514(Feb. 1983)

10. J.D. Klett, "Lidar Inversion with Variable Backscatter/Extinction Ratios," App. Opt., Vol.24, No.11, p.1638(Jun. 1985)

11. R.K. Measure, Laser Remote Sensing, New York: Willy-Interscience (1984).

12. G.J. Kunz, "Vertical Atmospheric Profiles Measured with Lidar," App. Opt.,Vol.22, No.13, p.1955(Jul. 1983)

13. J.M. Mulder, "Algorithm for Inverting Lidar Returns: Comment," App. Opt., Vol.23, No.17, p.2855(1984)

14. I.V.Samokhvalov, "Double-Scattering Approximation of Lidar Equation for Inhomogeneous Atmosphere," Optical Letters, Vol.4, No.1, p.12 (1979)

15. W.G. Tam, "Multiple Scattering Corrections for Atmospheric Aerosol Extinction Measurements," App. Opt., Vol19, No.13,

p.2090 (1980)

16. F.G. Fernald, B.M. Herman and J.A. Reagan, "Determination of Aerosol Height Distributions by Liadr," Journal of Applied Meteorology, Vol.11, p.482 (Apr. 1971)

17. H.G. Hughes, J. A. Ferguson, and D. H. Stephens, "Sensitivity of a Lidar Inversion Algorithm to Parameters Relating Atmospheric Backscattering and Extinction," App. Opt., Vol. 24, No. 11, p. 1609(Jun. 1985)

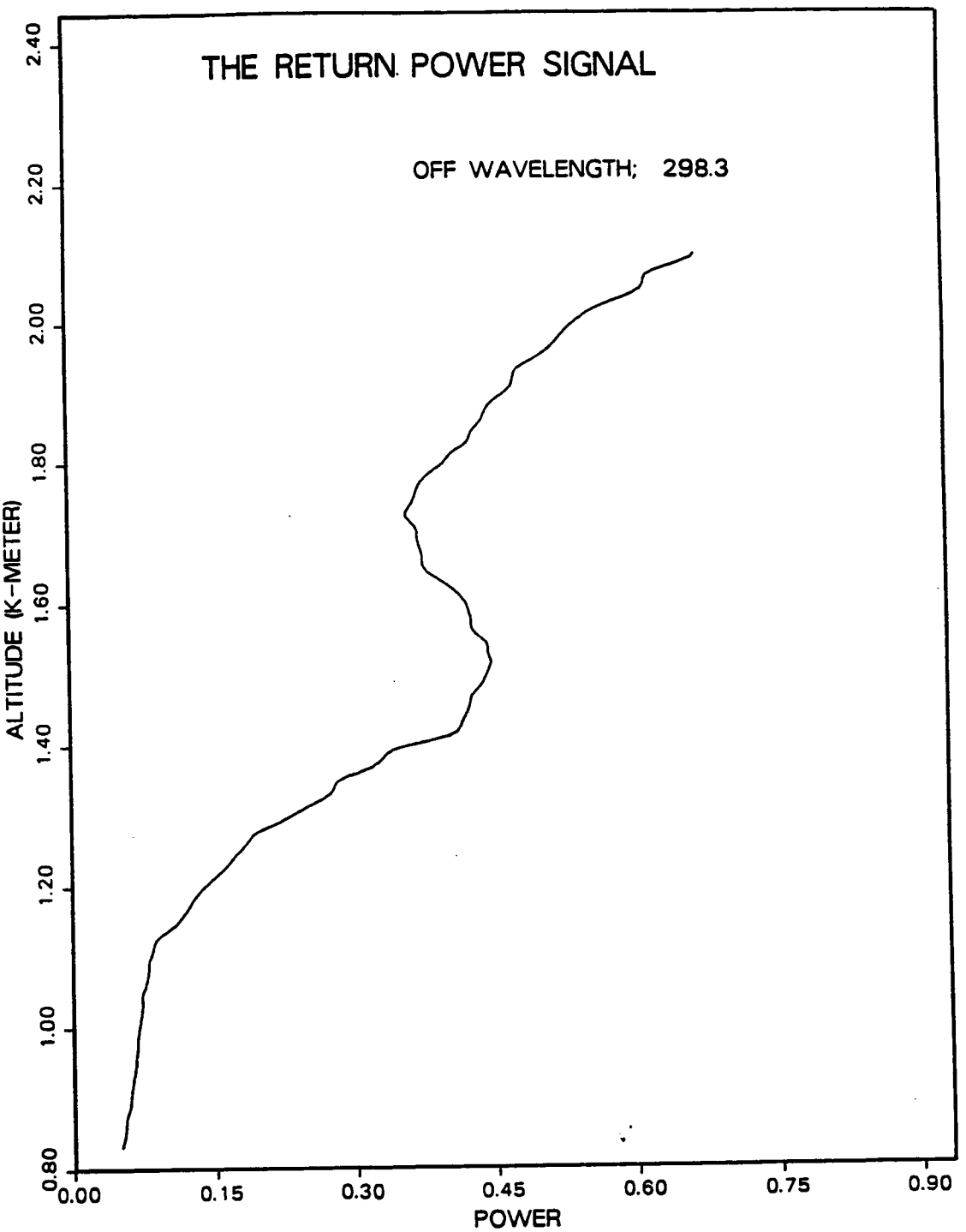

FIG. A THE RETURN POWER SIGNAL AT THE OFF WAVELENGTH

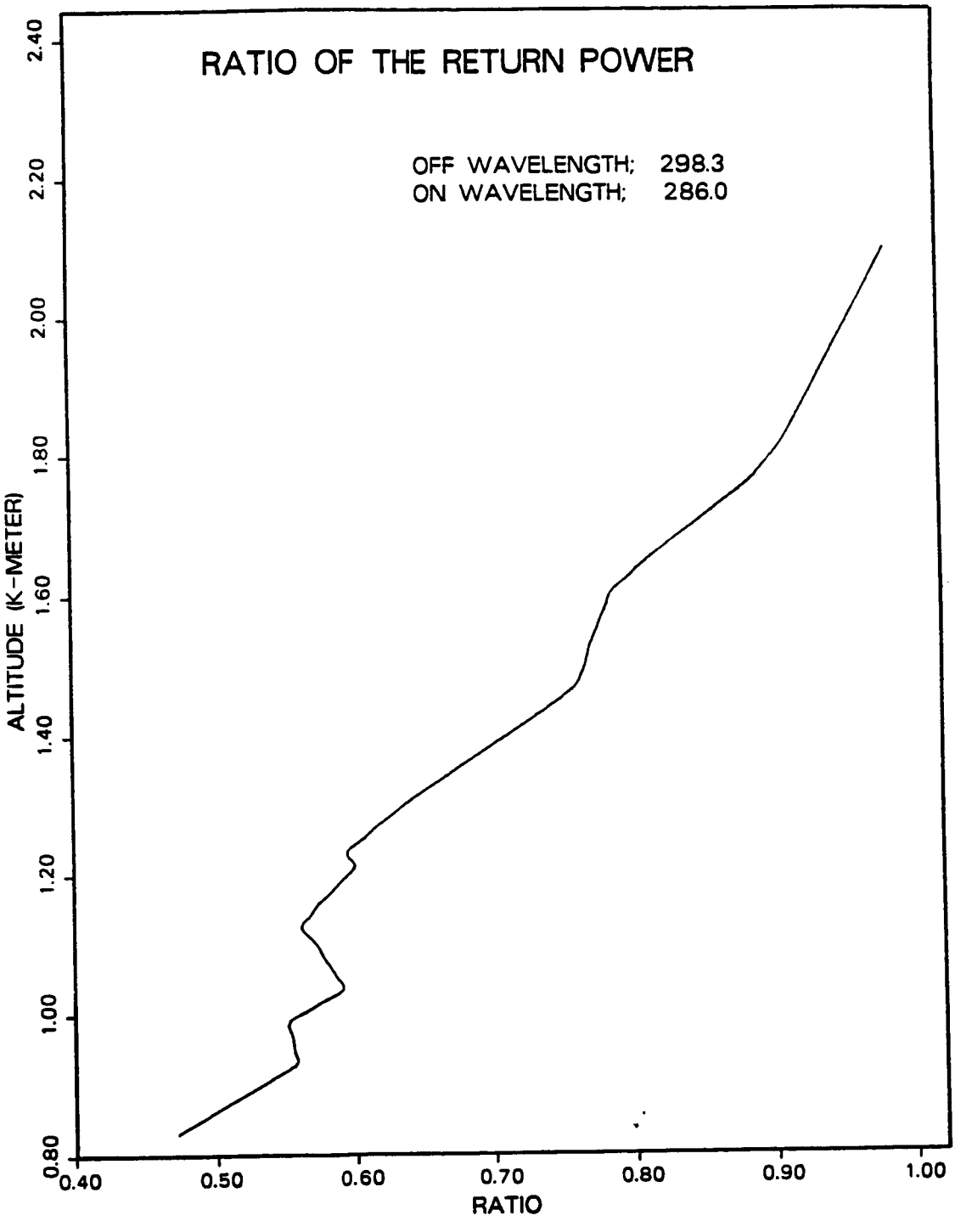

FIG. B RATIO OF THE RETURN POWER AT ON AND OFF WAVELENGTH

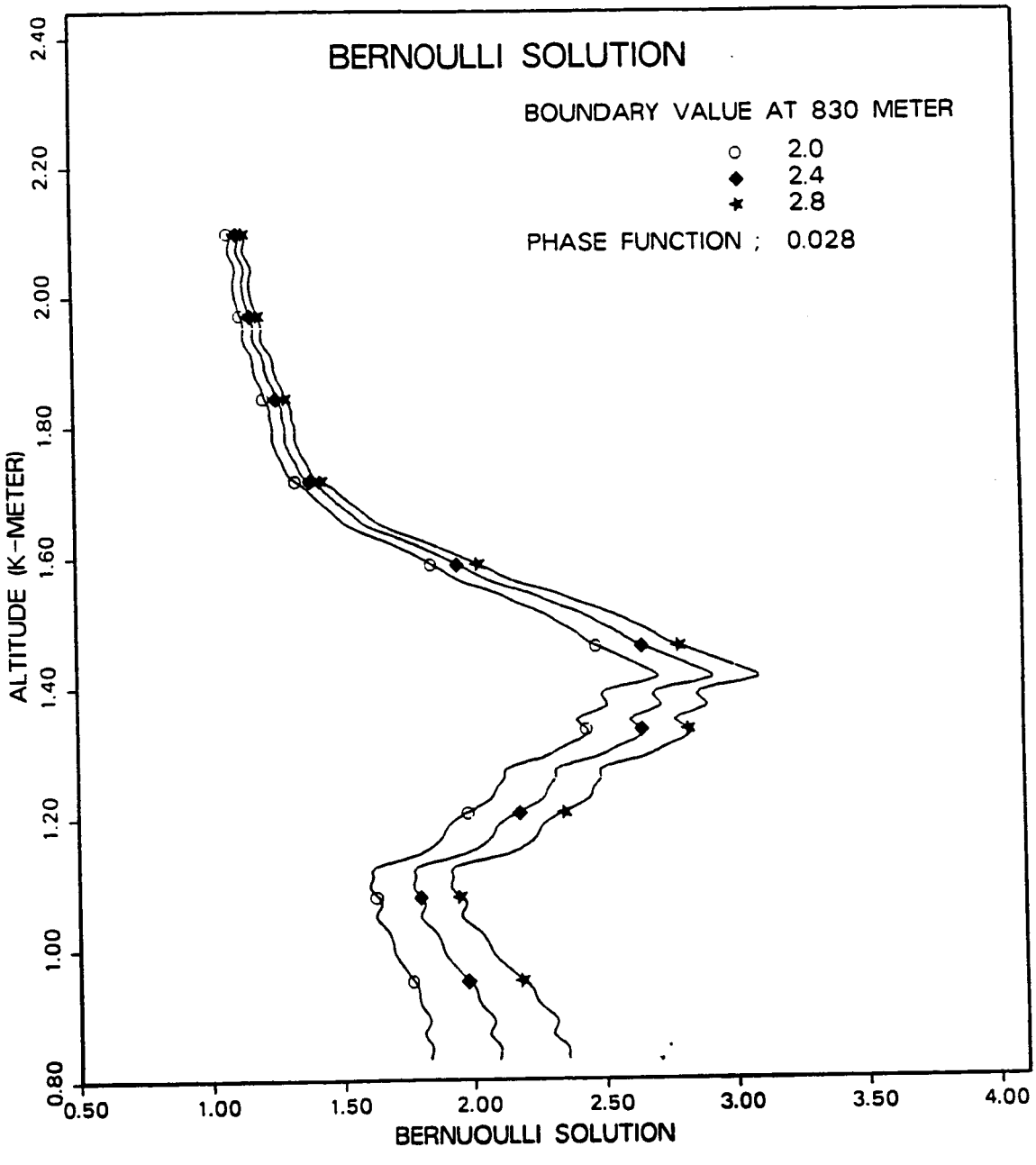

FIG. C BERNOULLI SOLUTION AT THE OFF WAVELENGTH (298.3)

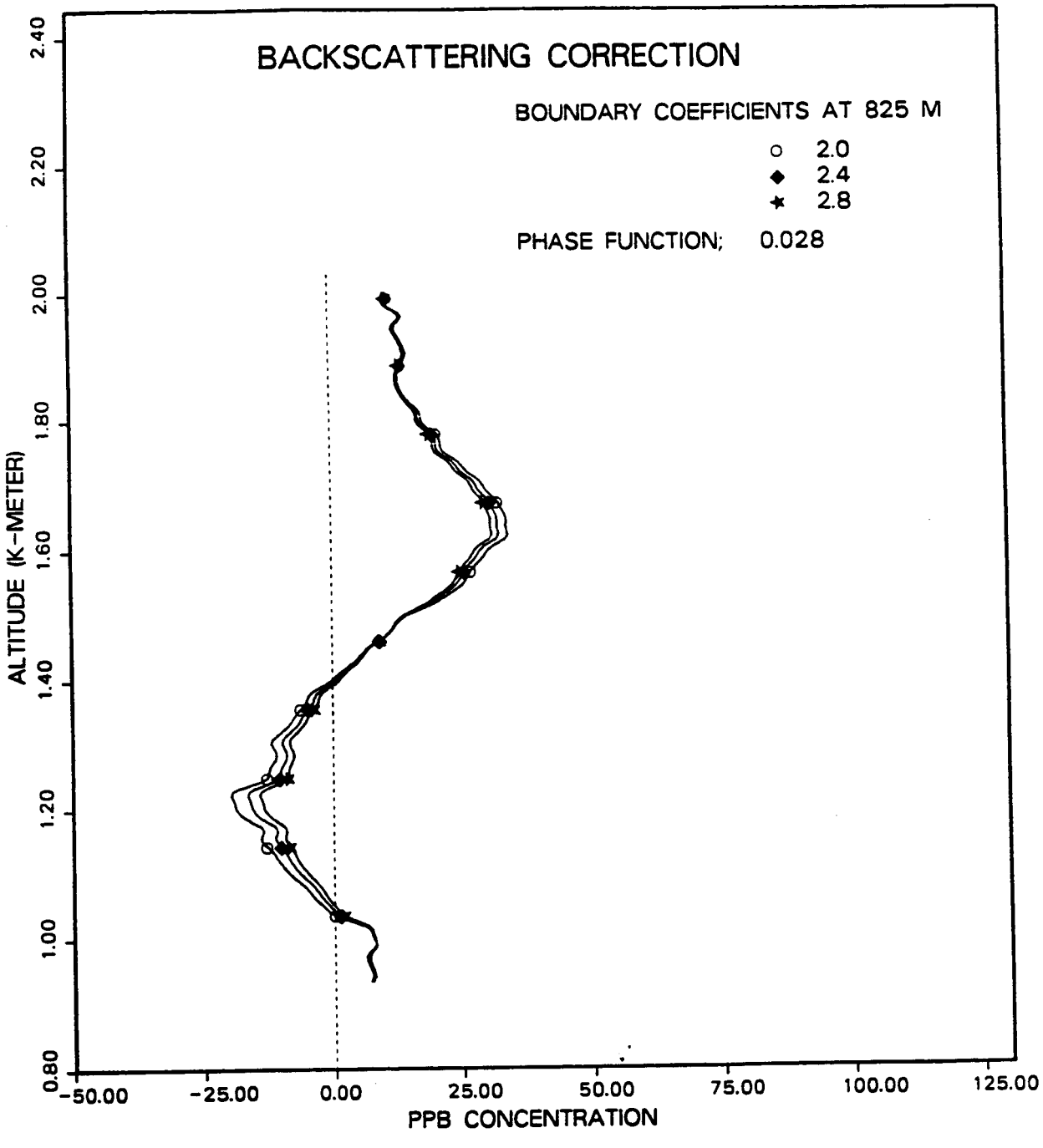

FIG. D BACKSCATTERING CORRECTION - PPB

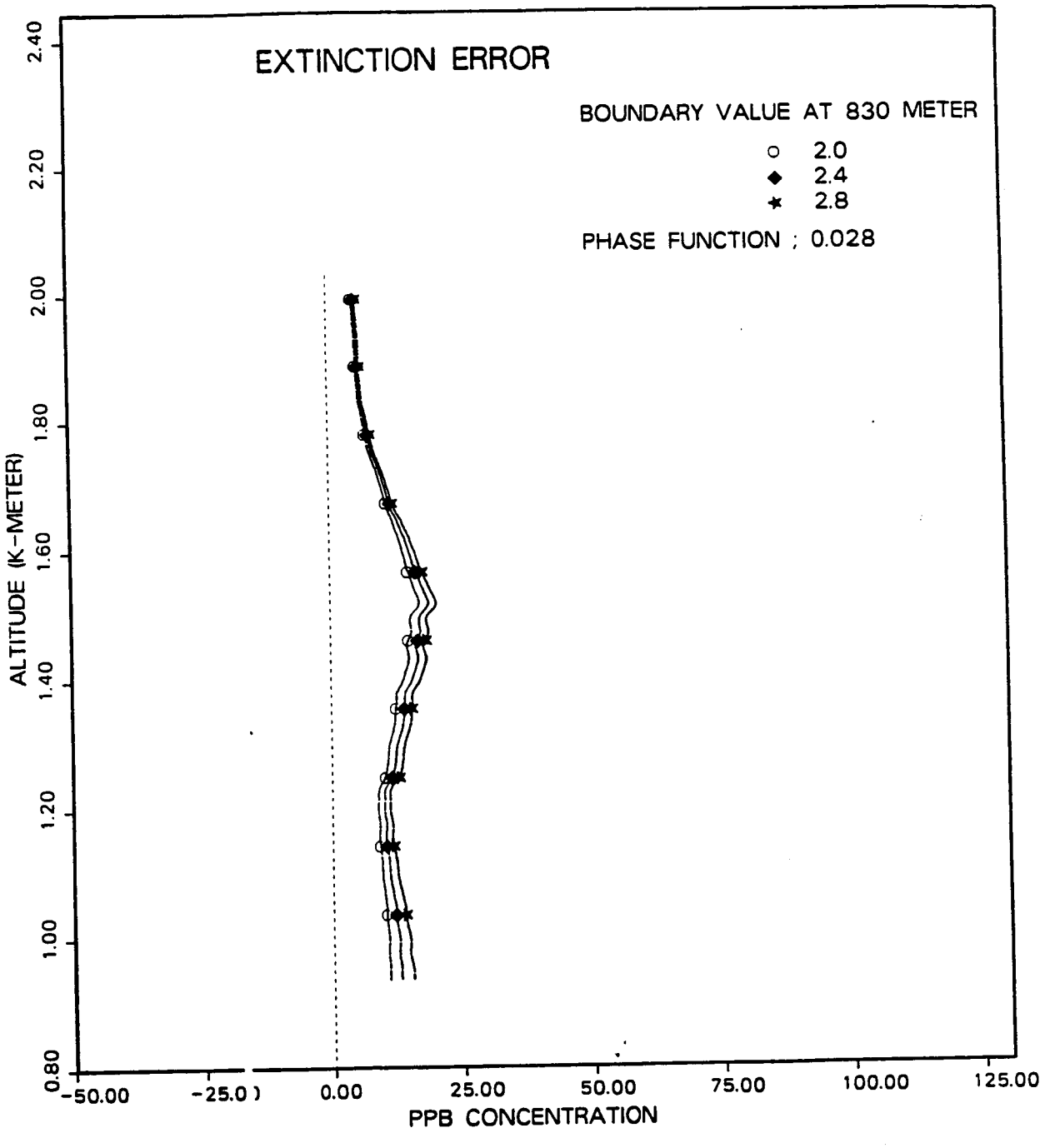

FIG. E EXTINCTION ERROR PROFILE - PPB

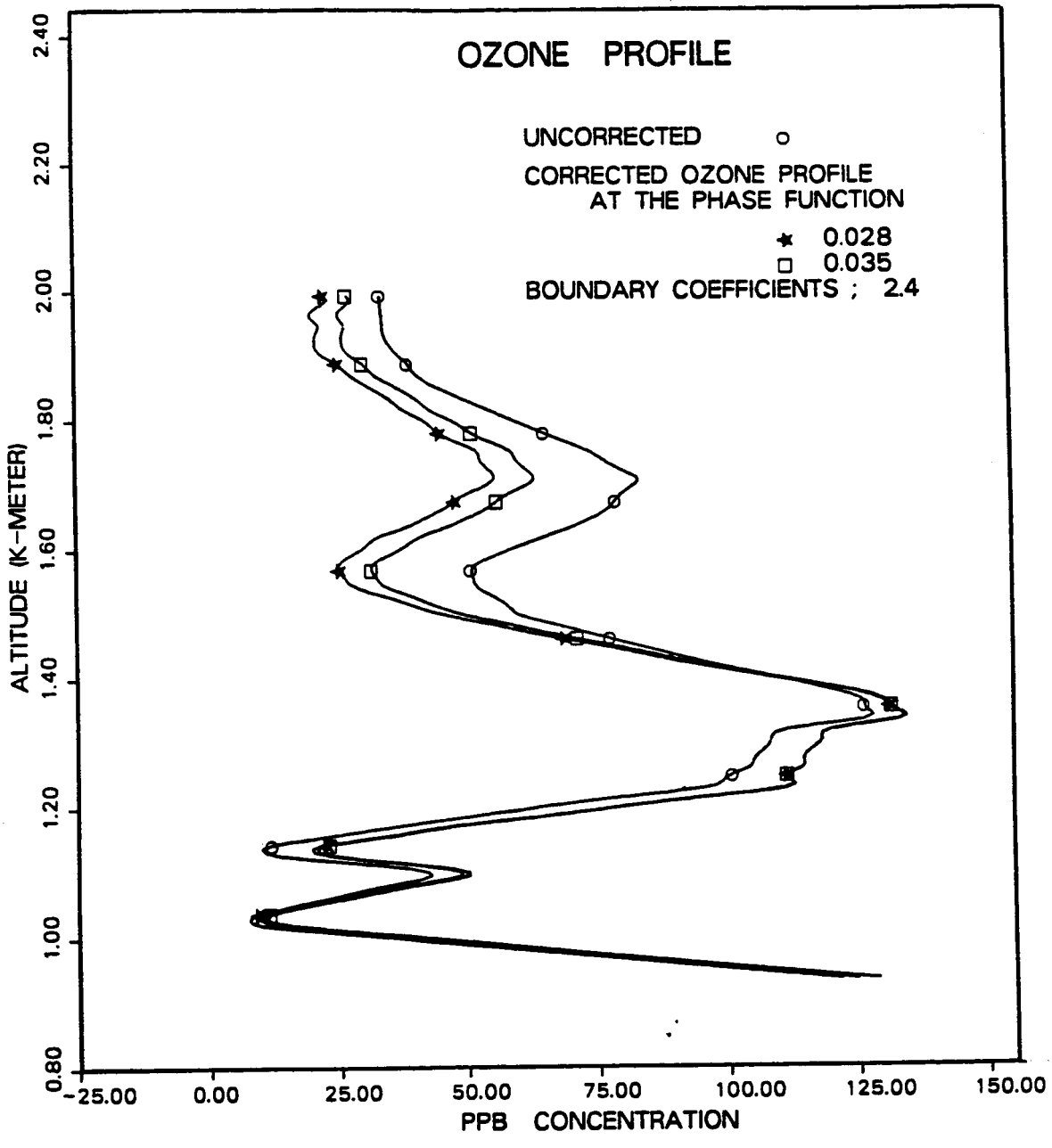

FIG. F UNCORRECTED AND CORRECTED OZONE PROFILE